MONOGRAPH 22

ATLAS OF NUCLEAR EMULSION MICROGRAPHS FROM PERSONNEL DOSIMETERS OF MANNED SPACE MISSIONS

Hermann J. Schaefer and Jeremiah J. Sullivan

NASA JOINT REPORT

27 May 1976

NAVAL AEROSPACE MEDICAL RESEARCH LABORATORY
PENSACOLA, FLORIDA 32508

Distribution of this document is unlimited.

ATLAS OF NUCLEAR EMULSION MICROGRAPHS FROM PERSONNEL DOSIMETERS OF MANNED SPACE MISSIONS

Hermann J. Schaefer and Jeremiah J. Sullivan

NASA Order No. T-3057C

Monograph-22

Approved By
Ashton Graybiel, M.D.
Assistant for Scientific Programs

Released By
Captain R.E. Mitchel, MC USN
Commanding Officer

27 May 1976

NAVAL AEROSPACE MEDICAL RESEARCH LABORATORY
PENSACOLA, FLORIDA 32508

FOREWORD

This monograph does not address itself to a specific research topic. It merely presents a collection of nuclear emulsion micrographs taken from selected missions of the era of manned space flights spanning th: years from Mercury to Apollo-Soyuz. It is an attempt to furnish a comprehensive illustration of the radiation environment in space as it manifests itself in nuclear emulsions of passive dosimeter packs carried by the astronauts on all missions. Main emphasis rests on the pictorial demonstration as such. Nuclear emulsion with its unique ability of faithfully recording the pathways of all ionizing particles penetrating it conveys even to the uninitiated observer at the microscope an immediate impression of the complex nature of the astronaut's radiation exposure in space. This atlas has been compiled as a permanent record furnishing the closest possible substitute for direct microscopic inspection of the flown emulsions.

Aside from its main purpose of official documentation, the atlas also serves well as a supplement to earlier reports and publicctions in which this laboratory has presented, throughout the years, the emulsion findings for individual missions. In view of these detailed accounts, the explanatory text preceding the picture section of the atlas is kept brief. The reader seeking detailed information on tissue-equivalent dosimetry with nuclear emulsion is referred to the earlier reports. A complete list is appended to the text section.

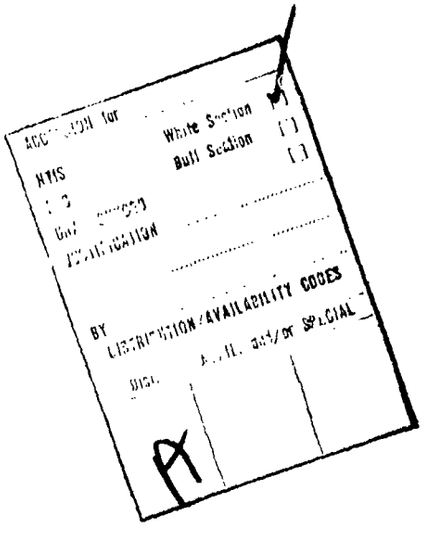

TABLE OF CONTENTS

INTRODUCTION 1

MERCURY MISSIONS 1

THE PROTON COMPONENT 2

HZE PARTICLES 4

DISINTEGRATION STARS 7

CONCLUSION 8

REFERENCES 8

TABLES 10

MICROGRAPHS 11

INTRODUCTION

The radiation environment in space is extremely complex. A large variety of nuclear particles, each kind, in turn, represented with a continuous energy spectrum, combines to a radiation which shows most intricate patterns of energy dissipation when it travels through matter. High energy primaries release, in vehicle frame and equipment and the body of the astronaut, numerous secondaries thereby altering profoundly the radiation field within the vehicle as compared to the incident radiation. Accordingly, measuring the astronaut's radiation exposure requires instruments directly on or at least in close proximity to the body. By this rationale, the astronauts carried, on all missions, dosimeter packs on their bodies containing a variety of passive radiation sensors, such as ordinary and nuclear emulsions, plastic foils, thermoluminescent (TLD) chips and neutron activation foils. Of these different recording media, the nuclear emulsions are unique inasmuch as they furnish under the microscope a complete pictorial record of all ionizing particles in the local radiation field. This atlas presents a collection of micrographs taken from nuclear emulsions flown on selected manned orbital and lunar missions. It shows the various kinds of nuclear particles which contribute to the astronaut's radiation exposure. Main emphasis rests on the visual demonstration as such. The explanatory text is kept brief. The sometimes intricate methods of determining by track and grain counts or analysis of other features of the microscopic image the astronaut's radiation exposure are not discussed in detail. The reader seeking basic information on the technique of tissue-equivalent dosimetry with nuclear emulsion is referred to earlier publications in which this laboratory has reported the findings on individual missions.

The atlas contains three different kinds of micrographs: 1) Normal "one-shot" pictures of visual fields as they appear in direct visual observation at the microscope without using the fine adjustment knob. 2) Sectional micrographs taken with a special camera equipped with two independent dark slides allowing consecutive partial exposures of the same negative film with the depth of sharp focus re-adjusted each time. 3) Panoramas of larger emulsion areas mounted together from component micrographs that are either one-shot or sectional pictures. Together, the three different types convey, as closely as this is possible with a still picture, the impression one obtains in direct microscopic observation.

MERCURY MISSIONS

Before beginning with a systematic illustration of the various components of the radiation field in space, it seems appropriate to present some micrographs from emulsions of the Mercury missions. Inasmuch as they are the first emulsions used for personnel radiation monitoring in space, they are of historical interest and should be preserved for the record.

The upper graph in Figure 1 is a low-power survey picture from an Ilford G.5 emulsion flown on Mercury-9. MA-9 was the last mission of the Mercury program with L.G. Cooper in "Faith 7" successfully completing 22 orbits in 34.3 hours on 15 May, 1963. On a background of numerous short tracks of trapped protons encountered in passes through the South Atlantic Anomaly, the micrograph shows one track of an HZE particle. A smaller section of the same heavy track, taken at higher magnification, is seen in the lower graph of Figure 1. The track has a strongly developed delta ray aura with some secondary electrons branching out as separate tracks to lateral distances of some 10 microns. These long delta rays characterize the track as produced by a so-called relativistic particle, i.e., a particle traveling at a speed approaching the speed of light.

Because of the short duration of the Mercury missions, tracks of heavy particles constitute infrequent events in the emulsions. A systematic illustration of the features of HZE particles can therefore not be compiled from the Mercury emulsions. However, Figure 2 conveys at least a general idea of the great diversity of the Z spectrum in showing four heavy tracks with different Z numbers estimated, from left to right, at 6-8, 8-10, 10-12 and 16-18. Again all tracks exhibit large delta ray auras indicating near-relativistic speeds of the particles. Characteristically, tracks of heavy primaries with small or vestigial auras are entirely absent in the Mercury emulsions owing to the fact that the near-Earth orbit of low geomagnetic inclination remained confined to a region of the magnetosphere to which low-energy galactic particles had no access.

Despite the scarcity of heavy tracks in the Mercury emulsions, one near-intersection of two HZE particle tracks occurred by coincidence in a G.5 emulsion flown on Mercury 8. The tracks are shown together in the upper low-power picture of Figure 3. Smaller sections of the two tracks are shown separately at higher power in the two lower pictures of the same figure. Z numbers of the tracks are estimated at 4-6 and about 20.

The statement that the inner regions of the magnetosphere are inaccessible for low-energy particles holds only for galactic radiation. Trapped protons originating from decaying neutrons within the magnetosphere itself show, quite differently, an energy spectrum centering heavily on low and very low energies. In a sensitive emulsion like the Ilford G.5 they produce mostly so-called black tracks, i.e., tracks of high grain density. Figure 4 shows four different visual fields with tracks of trapped protons. The two upper fields are taken from a G.5 emulsion flown on Mercury-8 (6 orbits) and show only a few proton tracks whereas the two lower fields taken from Mercury-9 (22 orbits) contain numerous tracks. The magnification of the micrographs in Figure 4 is too low for full resolution of the grain spacing in individual tracks. These aspects will be examined more closely in the next section.

THE PROTON COMPONENT

In any radiation exposure in free space, protons account for a major part of the total dose. While a sizeable number of protons originate locally in nuclear interactions of high-energy primaries in the matter of vehicle frame and equipment, trapped protons incident from the outside usually account for the larger share. On near-Earth orbital missions trapped protons are encountered in passes through the South Atlantic Anomaly. On deep space missions, only two brief exposures to trapped protons occur, one during trans-lunar injection and a second one in the terminal part of trans-Earth injection. Exposures of both kinds, anomaly passes and full traversals of the radiation belt, are characterized by essentially the same energy spectrum consisting of a continuum with the bulk of fluence contained in the interval from zero to about 300 Mev with a pronounced maximum in the 40 to 80 Mev region. Beyond 300 Mev the differential fluence rapidly drops to insignificant levels. Quantitative determination of absorbed dose and dose equivalent of the proton exposure, then, requires accurate determination of the spectrum from zero to at least 300 Mev corresponding to Linear Energy Transfer (LET) values from 90 to 0.3 kev/micron tissue.

The LET of a particle is reflected in the grain density of its track in emulsion. However, grain density is a strong function of LET only for a comparatively narrow interval. Therefore, one emulsion type or one degree of development can by far not cover the indicated LET interval for trapped protons with sustained accuracy of the grain count. The very sensitive Ilford G.5 emulsion in particular unless it is heavily underdeveloped, furnishes for the upper portion of the

LET spectrum tracks that are fully or nearly black. That means grain densities are so high that individual grains coalesce to blobs or continuous filaments. This is well demonstrated in Figure 5 which shows four selected sections of a so-called ender, i.e., the track of a proton entering the emulsion layer from outside yet coming to rest within. The proton traveled for 5.5 millimeters in the emulsion before it reached the end of its range. The section where it entered the emulsion is shown at the far right, the terminal section at the far left. The two center graphs show selected intermediate sections. Exact energy, range and LET data for the track sections displayed in Figure 5 are listed in Table I. Closer inspection of Figure 5 shows that accurate grain counting is quite difficult already for the track segment with the lowest grain density at the far right. Grain counting deteriorates all-together and becomes guess work for the remaining three downbeam sections.

The particle in Figure 5 entered the emulsion with an energy of 37 Mev corresponding to an LET of 1.6 kev/micron tissue. This energy lies in a region of the spectrum contributing most strongly to the total dose. A better grain resolution therefore appears essential. It could have been accomplished either by severe underdevelopment or by using an emulsion type of lower sensitivity. Either remedy, however, would have completely obliterated tracks at the upper end of the energy region of interest which still carries a sizeable portion of the total dose. It is seen, then, that the full spectrum cannot be resolved adequately with just one emulsion. This point is demonstrated in more detail in Figure 6 which shows four selected sections of a long proton ender in the less sensitive Eastman Kodak NTA emulsion. Table II lists ranges, energies and LET values. The superiority of the NTA over the G.5 for grain counting in the 30 Mev region is quite obvious. If good grain resolution is desired for still lower energies down to a few Mev, underdevelopment can be resorted to. Figure 7 demonstrates the effects which can be produced with various degrees of development on four different proton enders from slight overdevelopment at the far left to severe underdevelopment at the far right. It is seen that best resolution can be moved to any region up to the very maximum of the LET in the Bragg Peak. The price paid is of course a correspondingly higher cut-off LET below which the grain density becomes too small for a track to be recognized in the general background. The latter limitation is demonstrated in Figure 8 which shows the second ender from the left in Figure 7 in its full extension broken into five consecutive fractions. At its starting point at the upper end of the leftmost section, the proton had an energy of about 20 Mev corresponding to a residual range in emulsion of 1800 microns. It is quite evident that beginning at about that energy, tracks could be easily missed in the scanning process.

As seen from Figure 8, the minimum grain density at which a track is still identifiable strongly depends on the background of single grains from gamma rays and electrons. Angle of tilt of the track to the focal plane and, to a certain extent, scanning speed and experience of the observer are also factors. Therefore, specific limits of minimum grain densities and their corresponding LET values cannot be defined in general but have to be established individually for each set of emulsions. It is these circumstances that make quantitative work tedious and time-consuming. On the other hand, judicious adjustment of all factors ensures an accuracy that cannot easily be matched with any other dosimetric method.

The track in Figure 8 also demonstrates well the statistical variation of the mean number of grains per unit length. Grain density is usually quoted in terms of the number of grains per 100 micron emulsion. However, this does not mean that counting the grains on a 100 micron segment will always ensure satisfactory statistical significance. In most instances, substantially longer segments have to be counted for adequate statistics.

In a quantitative analysis of a continuous energy spectrum of protons as it is needed in space radiation dosimetry, the problem of reliable statistics is not limited to the grain count but imposes even higher demands of man-hours for microscopic scanning in regard to the number of track segments to be grain-counted in order to cover the energy spectrum. In terms of fluence, protons of very low energies constitute only a small fraction yet contribute, per particle, a disproportionately larger share to the total dose and all the more to the total dose equivalent than those of medium and high energies. In the scanning process, statistically significant numbers of the latter type segment accumulate much earlier than segments in the narrow energy band closely above zero. This circumstance places on a process, which is as such already quite time-consuming, the added burden of a useless accumulation of data on the fluence in one section of the spectrum before minimum statistical requirements in another section are fulfilled. It is therefore of paramount importance that the time requirements can be substantially reduced by combining the track and grain count analysis with a separate concomitant count of proton enders. The number of enders per unit volume of emulsion defines the differential fluence at low and very low energies, i.e., in a region contributing heavily to the total dose and all the more to the dose equivalent. At the same time, an ender count of satisfactory statistical significance requires much less scanning time than a track and grain count of the same accuracy. Especially in the less sensitive K.2 emulsion with its correspondingly smaller general background, proton enders stand out conspicuously allowing rapid scanning without impairing counting efficiency.

Figures 9 through 12 show typical micrographs containing two or more proton enders taken from K.2 emulsions flown on Apollo 6. Apollo 6 was a preparatory mission conducted mainly for testing the heat shield. Since it was an unmanned flight, it was purposely sent directly through the center of the inner radiation belt and carried an emulsion spectrometer. A total dose from protons in excess of 1.5 rad was recorded. The micrographs demonstrate that with moderate underdevelopment the K.2 emulsion maintains a comparatively low general background ensuring at the same time a grain density high enough for reliable identification of proton enders. Of special interest is Figure 10. It shows a field containing four proton enders, two of them of local origin from a disintegration star. Separate recording of star-produced enders and correcting the total count accordingly is essential for accurate determination of the low-energy section of the spectrum of trapped protons.

HZE PARTICLES

HZE particles are a unique component of space radiation with no counterpart in the terrestrial radiation environment. HZE stands for High Z number and Energy. The term was coined when the astronauts reported the eye flash phenomenon. It is a partial misnomer because it is actually the High Z but the Low E part of the galactic spectrum on which the very high LET values triggering the flashes center. Discovered in 1948 with nuclear emulsions flown in balloons at high altitudes, HZE (or better: HZLE) particles have fascinated ever since especially the cosmologist because they are believed to convey direct information on the abundance of the elements in the universe. Quite early, it also was realized that their mode of action on living matter should be quite different from all other types of nuclear radiations. Yet progress with actual biological experimentation has been slow so that even today radiobiological understanding of the "microbeam" effects of HZE particles in tissue is quite limited. On one hand, destruction of individual cells by a single passage of a heavy particle has been demonstrated. On the other hand, data on the general reaction to low levels of total body irradiation with HZE particles are completely missing. The complete lack of protection guides for HZE particles is expressly admitted in the recommendations of the International Committee on Radiological

Protection (ICRP). As the commission states, the dosimetric concepts for conventional radiations are not applicable to the "microbeam" exposure which HZE particles produce in tissue. Specifically, the dosimetric units rad and rem and the Quality Factor are completely inadequate for quantifying HZE particle exposure. Alternate new approaches to a quantitative assessment of acute or long term damage from HZE particle irradiation have not been proposed. In the absense of a dosimetric system and the presence of an urgent need for record keeping on radiation exposures in manned space operations, all that can be done is the recording of the basic physical parameters of exposure. As radiobiological knowledge, hopefully, will improve, it should eventually be possible to interpret such records in terms of the exposure status of the astronaut.

The primary galactic radiation contains particles of all Z numbers, each species represented with a continuous energy spectrum. The complex composition is reflected in a large variety of track configurations in nuclear emulsion. Interpretation of track structure in terms of Z, E and LET is an involved procedure. Accurate determination requires long track segments which are available only as a small percentage of the total track population in the thin stack of a few emulsion sheets of small size contained in a personnel dosimeter pack. An exposure record for the HZE particle component, therefore, can be established only in a semi-quantitative manner. Fortunately, particles with extremely high LET produce tracks with unique features that can be easily recognized. The fraction of the total fluence of HZE particles which constitutes the radiobiologically most significant component can therefore easily be identified in the scanning process and set apart from the remainder which can be measured in conventional dosimetric terms.

Figure 13 shows the terminal sections of six HZE particles with different Z numbers in K.2 emulsion. The characteristic dagger-like appearance with smooth contours is the important conspicuous clue for identifying events of extremely high LET. A particle reaches maximum LET always in the terminal section of its path shortly before it comes to rest. Since speed is low at that stage, the delta rays, although very numerous because of the high LET, are of short range. The two factors lead to a cross-sectional exposure distribution changing abruptly from saturation to zero thereby producing a solid black silver ribbon with sharp contours. However, the diameter of the track cannot be directly equated with LET because it is determined by the speed of the primary and not its LET. Because of their characteristic appearance suggesting a thinning out the terminal sections of HZE particle tracks are often called thindowns. The term is commonly used especially in the literature of the 50s and early 60s.

Particles of medium and high energies produce fewer delta rays, yet of higher ranges. As these secondary electrons branch out to the sides, the emulsion is no longer saturated in the more peripheral regions of the track and the tortuous trajectories of individual electrons (delta rays) become directly visible. This gives the track a fuzzy appearance which distinguishes it clearly from a low-energy, i.e., high-LET track. Figure 14 shows a set of six HZE particles of different Z numbers and high energies. Individual tracks of secondary electrons are clearly visible in the delta ray aura. Although density and lateral extension of the delta ray aura reflect LET and speed of the primary and thereby indirectly also its Z number, accurate Z and LET determination requires involved delta ray counts on longer track segments as mentioned above. The distinct difference between track segments with sharp convergent contours representing peak LET values and segments of lower LET with diffuse contours is demonstrated once more in a direct comparison of the two kinds of tracks in Figure 15. It is noteworthy that the LET for the track at the left is markedly higher than for the one at the right.

The transitional section of a heavy track where the delta ray aura shrinks and disappears is comparatively short for all Z numbers. The transition is especially rapid for higher Z numbers beginning at about Z ~ 20 because such very heavy nuclei lose more speed per unit length of path than lighter ones. Figures 16 and 17 convey an idea of how the microscopic image changes on a longer track segment of an Fe nucleus (Z ~ 26). Going upbeam from the point of termination of the track in the leftmost section in Figure 16, one recognizes that the delta ray aura develops rapidly on a short initial section but changes more slowly toward higher energies.

Because of the omnidirectional incidence of radiation in space, many tracks traverse the emulsion layer at a more or less large angle of tilt. As a consequence, a projective shortening of the microscopic image of a tilted track segment occurs which produces an apparent increase of the angle of convergence of the thindown contours for smooth tracks or of the density of the delta ray aura for fuzzy tracks. This optical distortion is further enhanced by a true shortening of a tilted track in the vertical dimension because of the shrinkage of the emulsion that occurs in processing. Since about half the total volume of unprocessed nuclear emulsion consists of silver bromide which is pactically all removed during fixation, the emulsion shrinks to about half its original thickness. It is seen by inspection that this shrinkage decreases the original angle of tilt and results in a true shortening of the original length of a tilted track segment. Therefore, tilting the emulsion sheet under the microscope back to a position where a track would be parallel to the focal plane of the objective can only rectify the optical distortion but not the true shortening due to emulsion shrinkage.

For larger angles of tilt, the image distortion due to the two indicated effects is considerable. For tilted smooth tracks, the contours converge more rapidly. For fuzzy tracks, the delta ray aura appears more dense. Both effects can easily lead to overestimates of Z and LET. As far as smooth tracks are concerned, a precise determination of the complete geometry including the verticle dimension allows a reconstruction of the undistorted track although at the price of a tedious procedure. The artificial increase of the density of the delta ray aura for fuzzy tracks could only be corrected with an anamorphic lens.

Examples of heavily tilted tracks are shown in Figures 18, 19 and 20. Figure 18 shows at the left a low-power survey picture of two heavy tracks in a 100μ K.2 emulsion. The micrograph was taken with the emulsion sheet tilted toward the focal plane so that the pre-thindown was in focus with its full length. The center and right picture are sectional micrographs showing the two tracks separately at higher magnification. Figure 19 shows an almost complete thindown of an estimated Z > 20 again with the emulsion tilted in order to bring the full length of the segment into focus. Figure 20 shows two short thindowns that barely dipped into the emulsion. Such short steep track segments are very elusive and easily missed in the scanning process because, with the emulsion parallel to the focal plane, only a small part of the total segment is in focus at one time. Therefore, the picture seen in the microscope does not at all offer the clarity of the micrographs in Figure 20 taken with the tracks parallel to the focal plane. The buckling of the two tracks in Figure 20 is an artefact produced by emulsion shrinkage in fixation which forces a contraction upon the silver ribbon embedded in the gelatin.

For operational dosimetry of HZE particle exposure in space, the analysis of the individual event of local passage of an HZE particle is not the only issue. Of equal or maybe even greater importance is the assessment of effects from total body irradiation. At present no experimental data are available on this particular issue. Since hit frequencies from HZE particles are comparatively small even for mission times of 10 or more days, the distribution of hits in the microstructure of tissue shows pronounced statistical variations. Scanning emulsions at low power, one encounters

fields almost devoid of HZE particle events alternating irregularly with others showing clusters of heavy tracks according to the laws of the Poisson Distribution. It appears of interest to present some low power micrographs of emulsion areas with unusual clustering of HZE particles illustrating cases at the upper end of the Poisson Distribution. Figure 21 shows a panorama mounted together from several fields taken from a 100μ K.2 emulsion flown on Apollo 17. Field size is 773 x 378 microns. Figure 22 shows another panorama from the same mission. Field size is 906 x 367 microns. The three heaviest tracks are numbered and shown separately at higher magnification in Figure 23. It should be noted that the intersection of tracks 2 and 3 in Figure 22 is not real. Direct visual observation at very high power under the microscope reveals a vertical emulsion distance of 12 microns. In fact, we have seen, in the rather large emulsion material from all Apollo flights, only very few intersections with both partners heavier than Z = 10 that could not be resolved even with a 100x objective. In other words, double hits of HZE particles in space are extremely rare.

Figure 24 shows a circular field taken at very low power (10x objective and 5x eye piece) directly as it appears in visual observation under the microscope. Again, the heavy clustering of several HZE particles in one field is unusual. Four tracks are numbered and shown again at higher magnification in Figure 25. Figures 26 and 27 show 3 more circular fields demonstrating the two different magnifications as we apply them in routine scanning of HZE particles. For best time economy, a first run covering the entire emulsion sheet is conducted at low power as shown in Figure 26. In this run, Z numbers and delta ray auras of heavy tracks are roughly estimated and stage micrometer coordinates recorded to ensure quick re-focussing for final grading in the second run at higher power as shown in Figure 27.

While panorama micrographs taken at low power illustrate well the low frequency and random distribution of heavy events, they do not allow reliable Z and LET estimates. The assembly of panorama pictures from component fields taken at higher power, on the other hand, is a cumbersome task quite similar to a jigsaw puzzle with the added hindrance that the low depth of focus distorts and sometimes completely obliterates the clues for aligning the pieces. However, such assemblies are essential for a more accurate microdosimetric mapping of the radiation field in a cluster area as the radiobiologist would need it for assessing the effects on cellular systems. In order to cut the work load to size in preparing such panoramas, we have limited the depicted areas strictly to the regions containing the track configurations of interest with no regard for the irregular and sometimes weird shapes of the finished assemblies.

Figures 28 through 34 show panoramas of emulsion areas containing clusters of heavy tracks taken at high magnification. Because of the low depth of focus even the component fields had to be shot as sectional micrographs with the special camera described earlier. In some instances adjacent component fields had to be taken at such greatly different depths within the emulsion that no coherent background grain configurations bridging the seams are apparent in the pictures. It should be pointed out that even in these cases precise alignment has been accomplished by superpositioning the uncropped negatives and cutting them simultaneously.

DISINTEGRATION STARS

A more detailed evaluation of the radiation fields shown in the panoramas is not attempted here. The reader desiring quantitative data on the LET values of various tracks is referred to Figures 13 and 14 for LET estimates. The fields shown in Figures 33 and 34 contain, besides HZE particle tracks, also large disintegration stars. Since multipronged stars can originate only from nuclear disintegrations of heavy elements, specifically silver and bromine in nuclear emulsion,

they are not representative of tissue. However, stars released in the gelatin matrix of the emulsion do reflect the tissue dose. Such stars are recognized by their smaller prong numbers according to the low Z numbers of the constituent elements of gelatin. Figures 35 through 37 show such gelatin stars in K.2 emulsion. Tissue disintegration stars furnish a sizeable contribution to the mission dose equivalent firstly because they are a prolific source of low-energy protons and alpha particles and secondly because they constitute the main source of neutrons which in turn account for a high-LET component of the mission dose produced by recoil protons. For a more detailed discussion of how the two contributions can be assessed from the prong spectrum of the total star population in emulsion the reader is referred to earlier publications.

CONCLUSIONS

At the conclusion of the brief comments to the collection of micrographs, it should be pointed out once more that a photomicrograph even if taken with the sectional camera is a poor substitute for direct observation with the microscope where the observer can continuously adjust the plane of sharp focus with the fine adjustment knob. Workers in the field interested in such direct examinations for further exploitation of the large volume of unretrieved data still buried in the emulsions should arrange, with the Lyndon B. Johnson Space Center, for obtaining emulsions on loan. Re-examination of specific events shown in this atlas is easily accomplished by relating the stage coordinates marked on each picture to those of a reference mark furnished with each emulsion sheet.

REFERENCES

1. Schaefer, H.J., and Sullivan, J.J., Measurements of the astronauts' radiation exposure with nuclear emulsion on Mercury Missions MA-8 and MA-9. NSAM-896. NASA Manned Spacecraft Center. Pensacola, Florida: Naval School of Aviation Medicine, 1964.

2. Schaefer, H.J., Linear energy transfer spectrum of proton exposure on Mercury Mission MA-9. NSAM-899. NASA Order R-75. Pensacola, Florida: Naval School of Aviation Medicine, 1964.

3. Schaefer, H.J., Radiation monitoring on Project Mercury: Results and Implications. Aerospace Med., 35: 829-833, 1964.

4. Schaefer, H.J., and Sullivan, J.J., Radiation monitoring with nuclear emulsions on Project Gemini. I. Experimental design and evaluation procedure: Partial results on Missions 4 and 5. NAMI-955. NASA Manned Spacecraft Center. Pensacola, Florida: Naval Aerospace Medical Institute, 1966.

5. Schaefer, H.J., and Sullivan, J.J., Radiation monitoring with nuclear emulsions on Project Gemini. II. Results on the 14-day Mission Gemini VII. NAMI-990. NASA Manned Spacecraft Center. Pensacola, Florida: Naval Aerospace Medical Institute, 1967.

6. Schaefer, H.J., and Sullivan, J.J., Radiation monitoring with nuclear emulsions on Project Gemini. III. The flux of galactic heavy primaries on Gemini VII. NAMI-1017. NASA Manned Spacecraft Center. NAMI, 1967.

7. Schaefer, H.J., and Sullivan, J.J., Radiation monitoring with nuclear emulsions on Mission Gemini IV and V. Aerospace Med., 38: 1-5, 1967.

8. Schaefer, H.J., Messungen der Protonendosis der Gemini-Astronauten mit Kernemulsionen. Biophysik., 4: 63-76, 1967.

9. Schaefer, H.J., and Sullivan, J.J., Nuclear emulsion measurements of the astronauts' radiation exposure on Apollo VII. NAMI-1060. NASA Manned Spacecraft Center. Pensacola, Florida: Naval Aerospace Medical Institute, 1969.

10. Schaefer, H.J., and Sullivan, J.J., Nuclear emulsion recordings of heavy primaries on Apollo VII and VIII. NAMI-1091. NASA Manned Spacecraft Center. Pensacola, Florida: Naval Aerospace Medical Institute, 1969.

11. Schaefer, H.J., and Sullivan, J.J., and Richmond, R.G., Dosimetry of proton radiation fields in space with nuclear emulsions. Health Phys., 19: 663-670, 1970.

12. Schaefer, H.J., and Sullivan, J.J., Nuclear emulsion recordings of the astronauts' radiation exposure on the first lunar landing mission Apollo XI. NAMRL-1112. NASA Manned Spacecraft Center, Pensacola, Florida: Naval Aerospace Medical Research Laboratory, 1970.

13. Schaefer, H.J., Benton, E.V., Henke, R.P., and Sullivan, J.J., Nuclear track recordings of the Astronauts' radiation exposure on the first lunar landing mission Apollo XI. Rad. Rsch., 49: 245-271, 1972.

14. Schaefer, H.J., Microdosimetric Structure of HZE particle tracks in tissue. NAMRL-1214. Naval Aerospace Medical Research Laboratory, 1975.

TABLE I

Positions: #	Residual Range, microns Em	Energy Mev	LET kev/micron Em
A	516	9.50	10.9
B	2100	21.5	5.85
C	4200	32.0	4.30
D	5500	37.0	3.85

See Figure 5.

TABLE II

Positions: #	Residual Range, microns Em	Energy Mev	LET kev/micron Em
A	200	5.4	16.3
B	1850	20	6.20
C	3550	29	4.60
D	4860	35	4.00

See Figure 6.

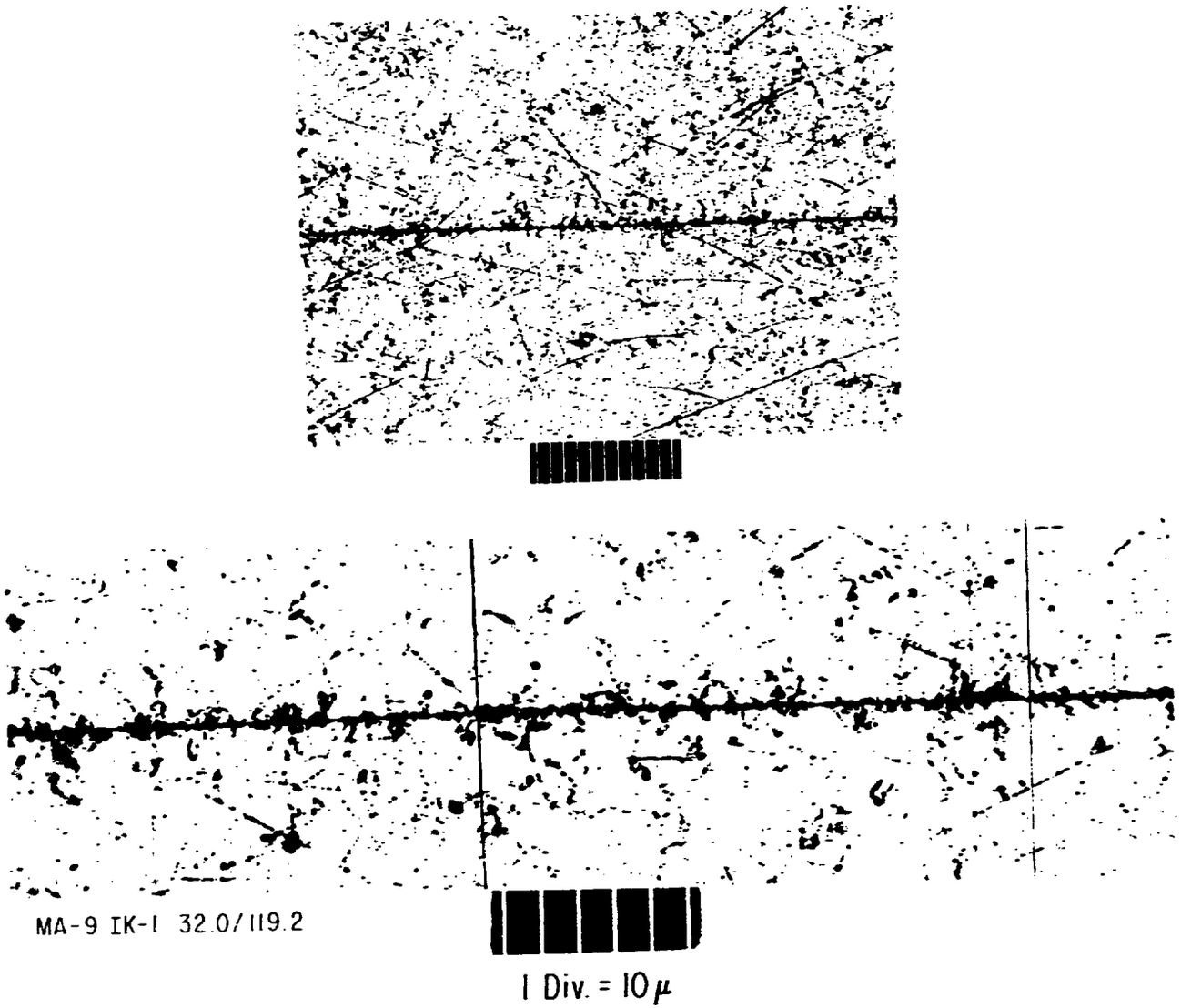

Mercury 9 50 μ G.5

Heavy Track Z_{est} = 18 at Two Different Magnifications

Figure 1

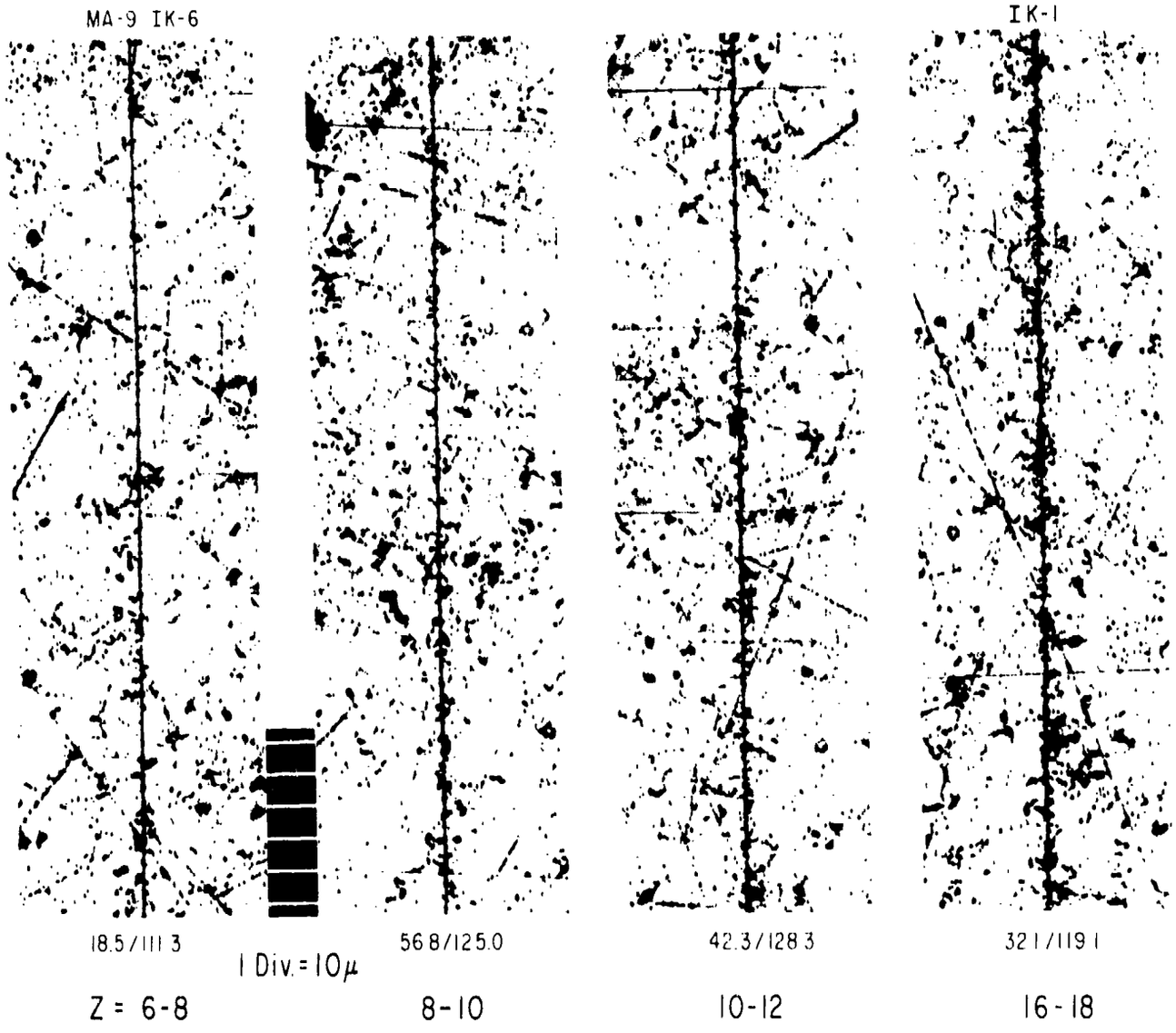

Mercury 9 50μ G.5
Four Heavy Tracks of Different Z - Numbers

Figure 2

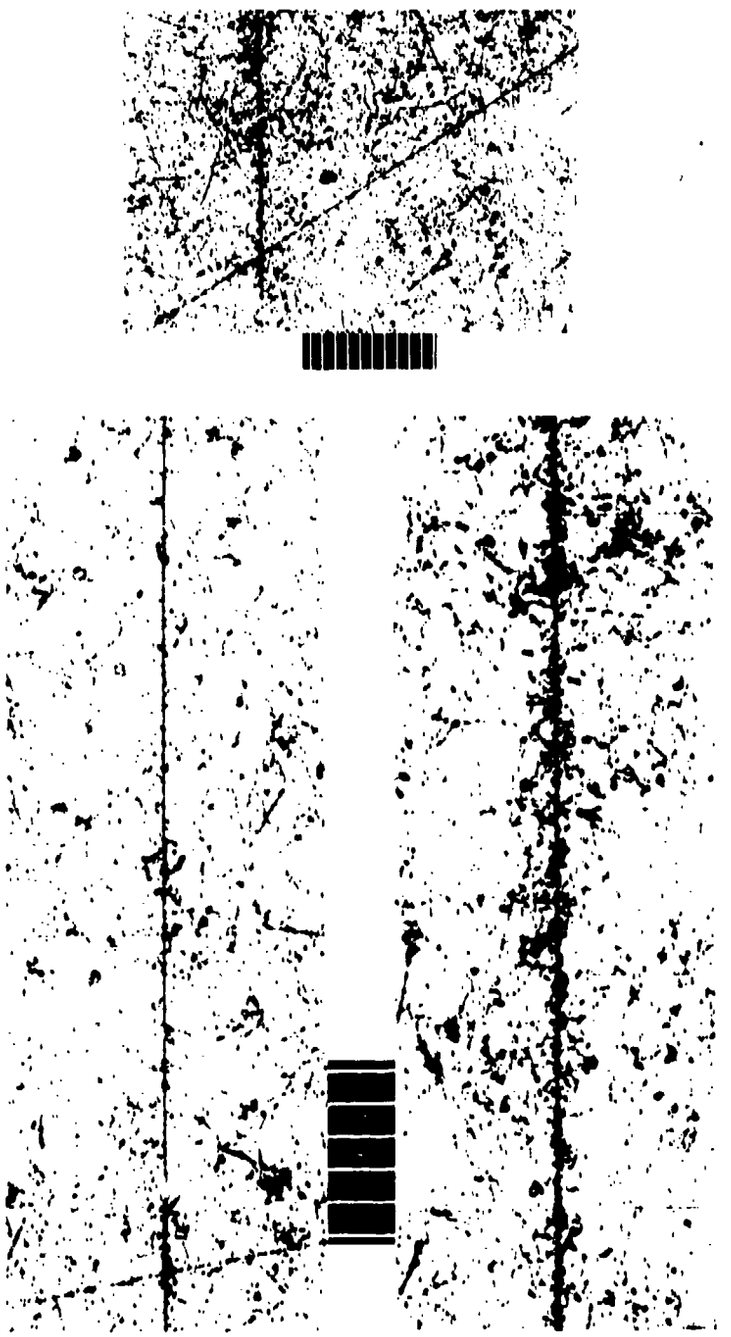

1 Div. = 10 μ

Mercury 8 50μ G.5
Near-Intersection of Two Heavy Tracks
Z = 6-8 and 20

Figure 3

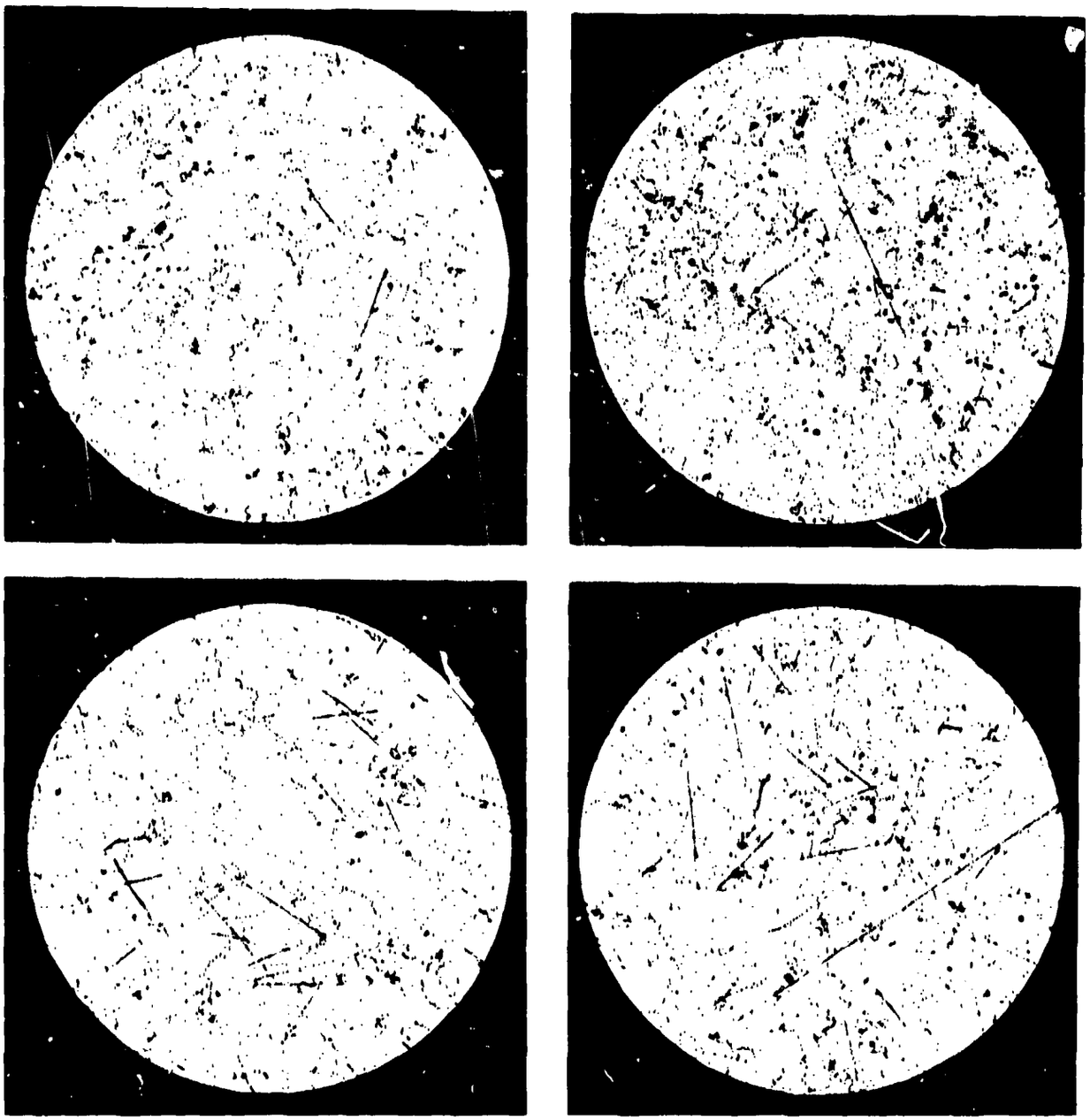

Random Fields With Tracks of Trapped Protons
Upper : Mercury 8 50μ G.5 IIY-6
Lower : Mercury 9 50μ G.5 IK-6
Diameter of Field : 275μ

Figure 4

Selected Sections of Proton Ender in Ilford G5 Emulsion Flown on Mercury 8
Residual Ranges, Microns Em

A: 530 B: 2100 C: 4200 D: 5500

Figure 5

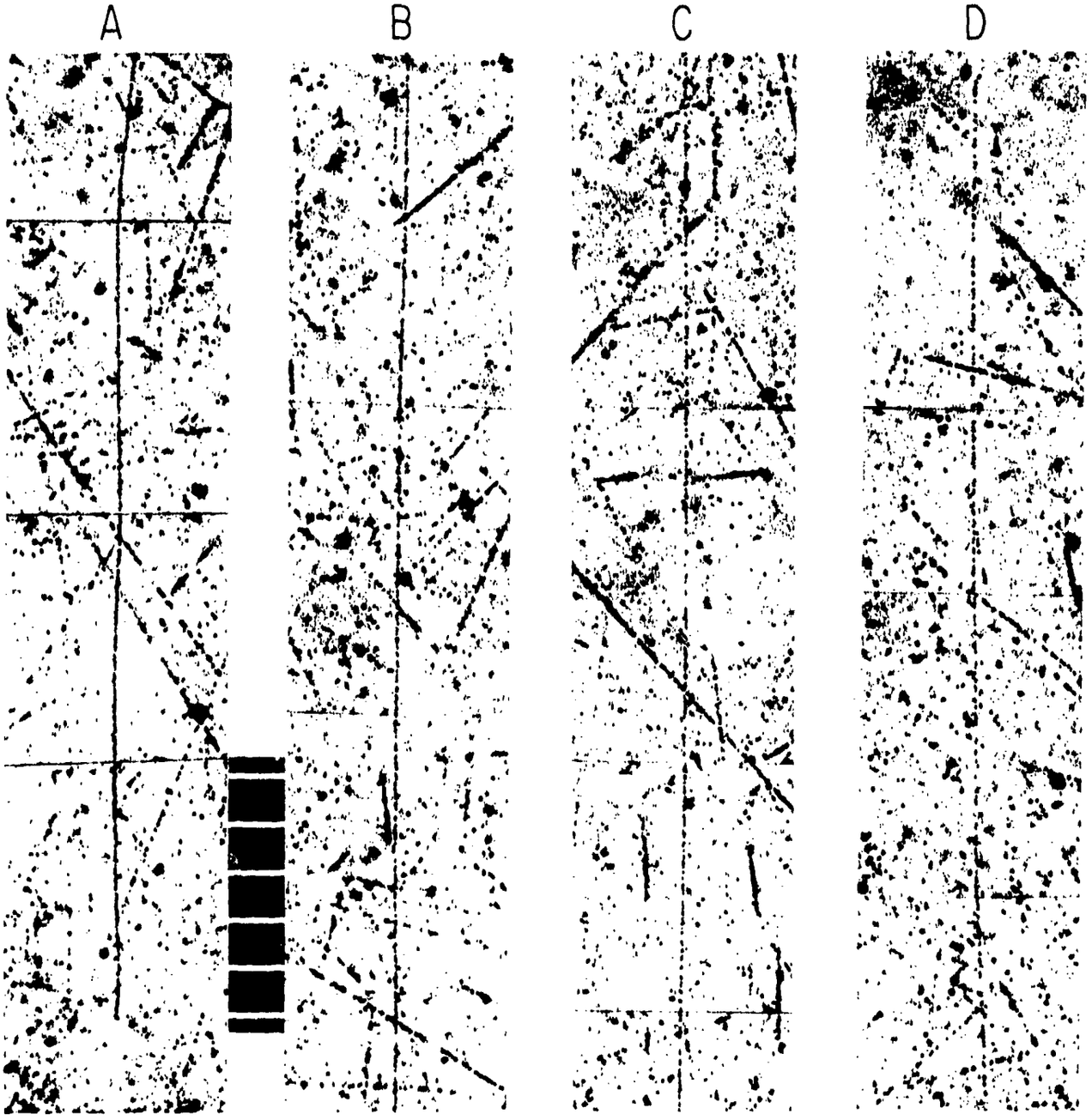

Proton Ender In Eastman Kodak NTA Emulsion Flown On Apollo 4

Residual Range, microns Em:
A200 B1850 C3550 D 4860

Figure 6

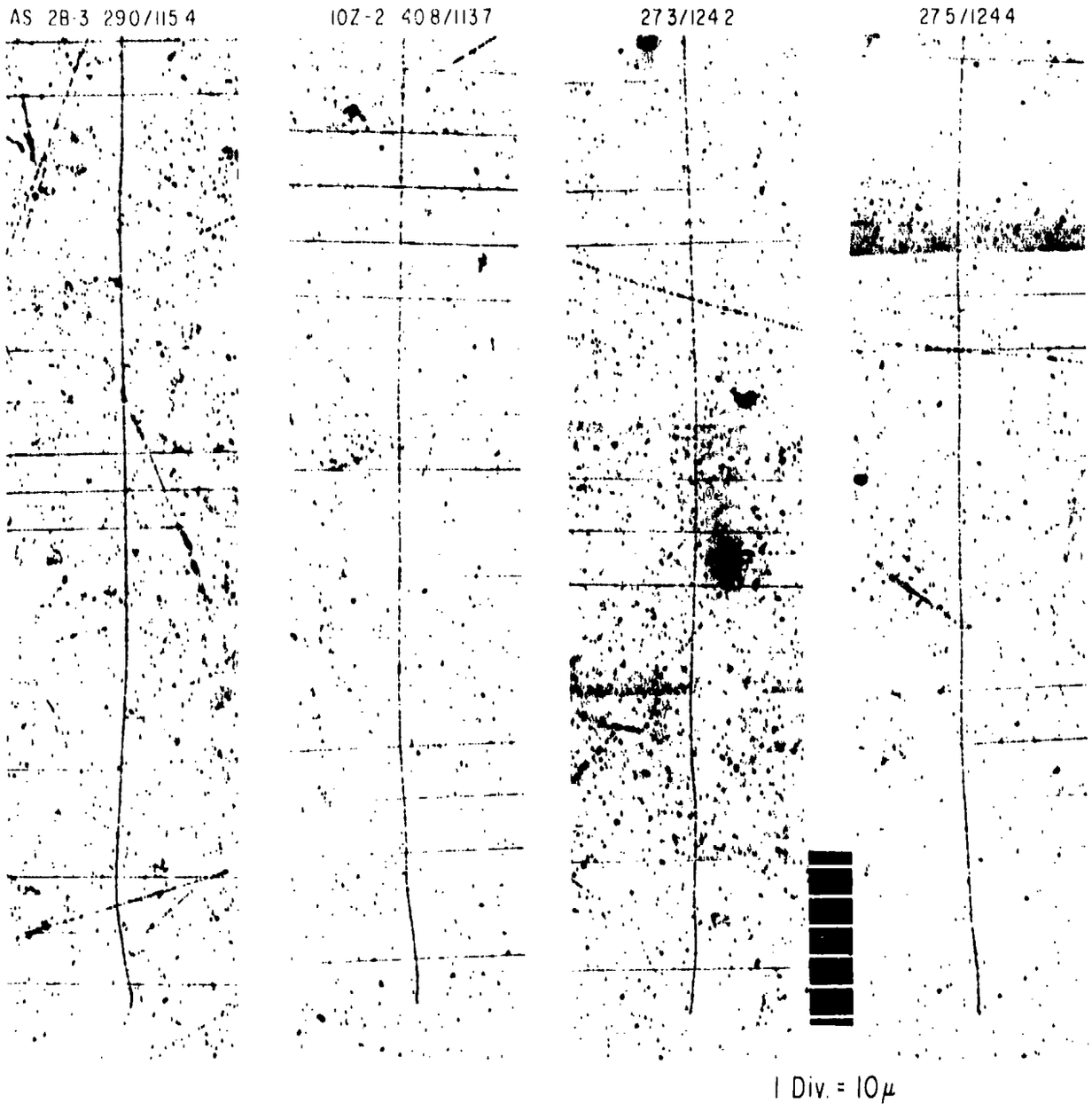

Proton Enders in 100μ K.2 Emulsions Flown on Apollo 7 Showing Four Different Degrees of Development

Figure 7

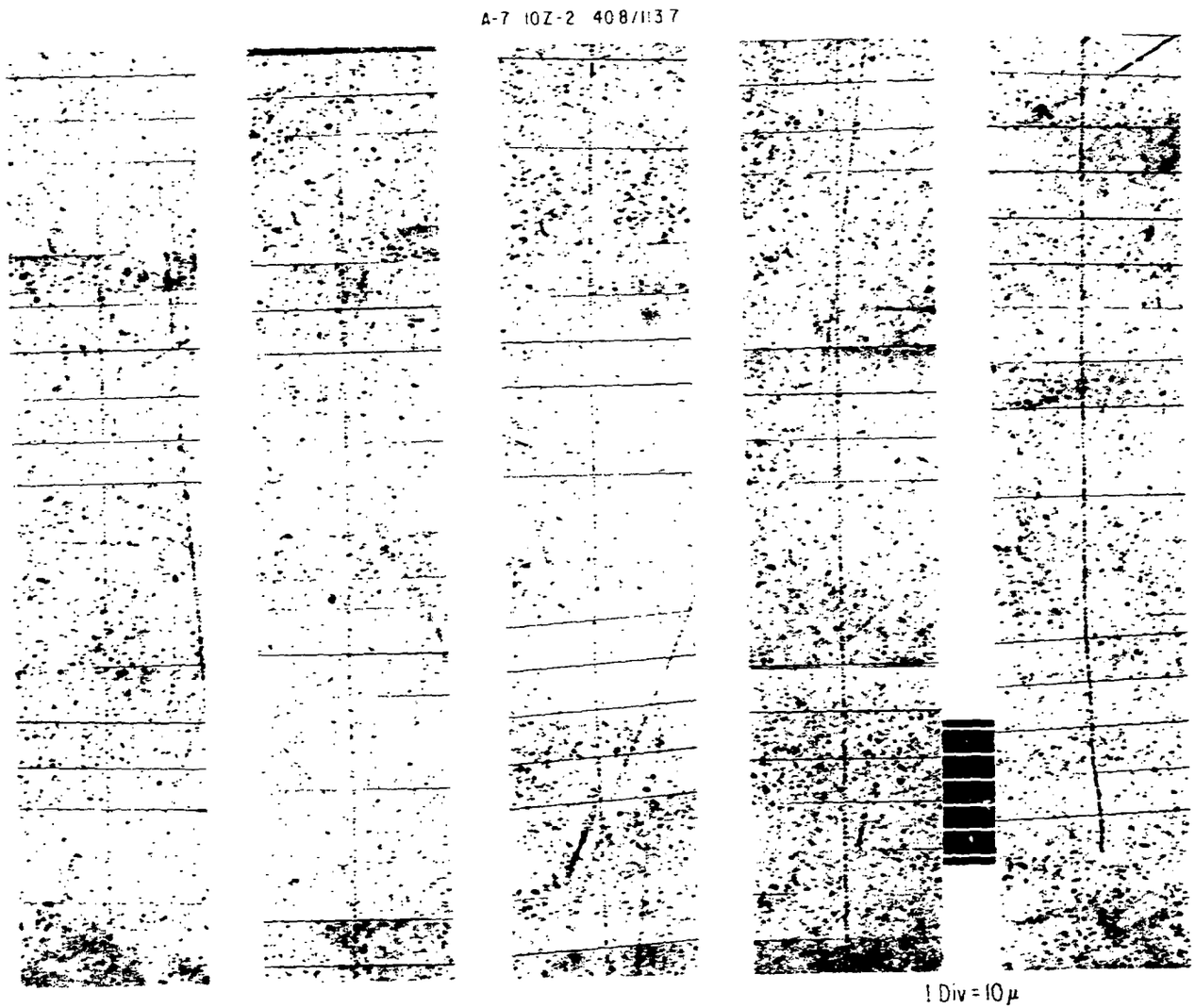

Apollo 7 100μ K.2
Consecutive Sections of Long Proton Ender

Figure 8

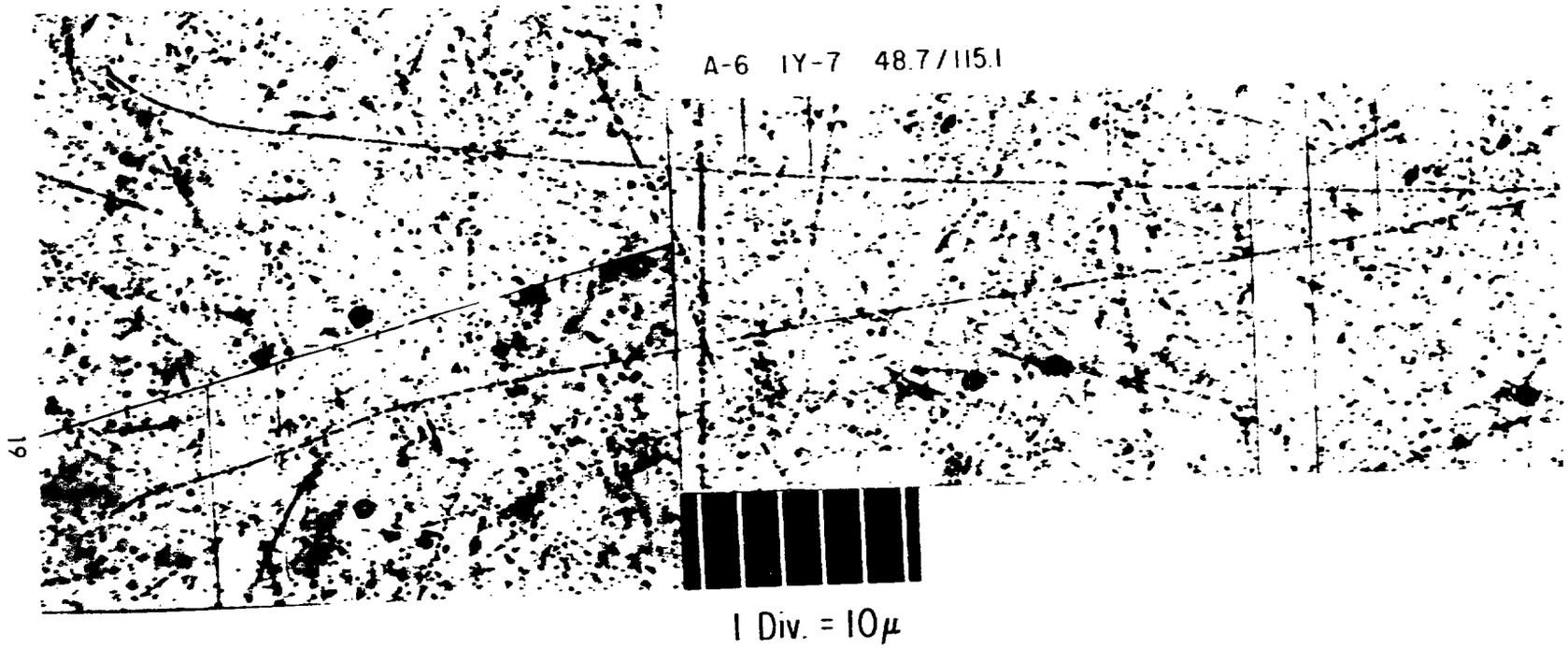

Proton Enders Apollo 6 100μ K.2

Figure 9

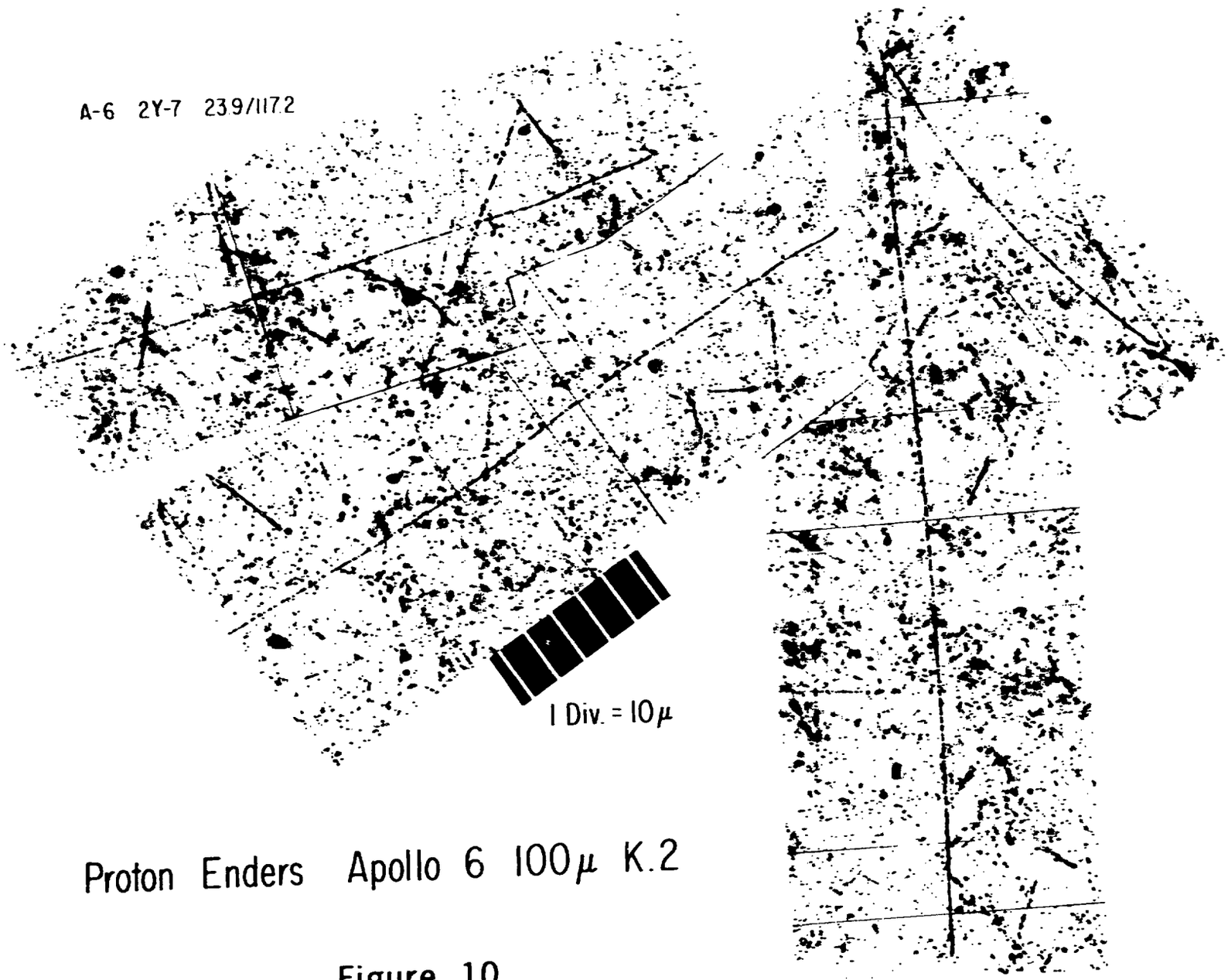

Proton Enders Apollo 6 100μ K.2

Figure 10

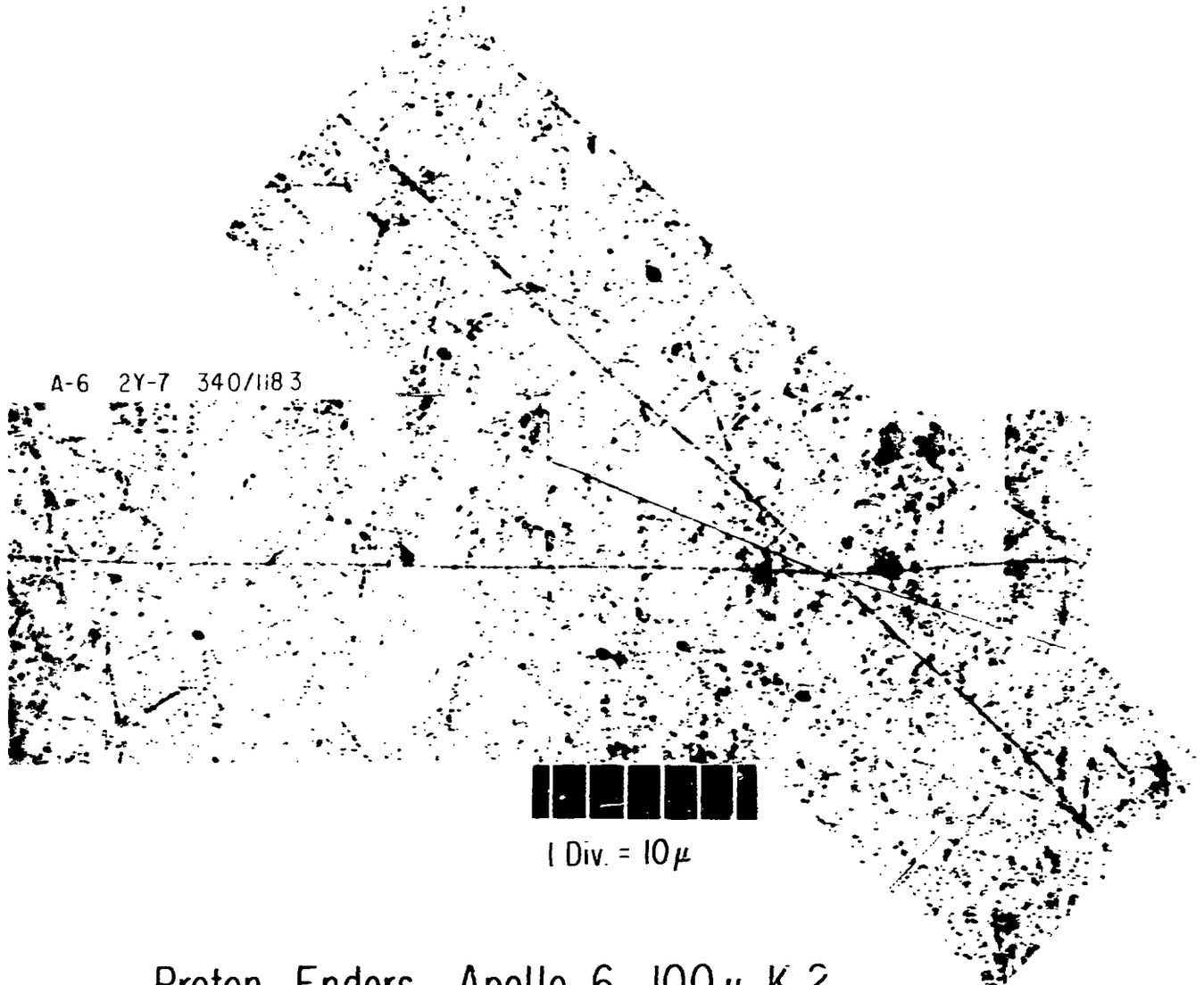

Proton Enders Apollo 6 100μ K.2

Figure 11

Proton Enders Apollo 6 100 μ K.2

Figure 12

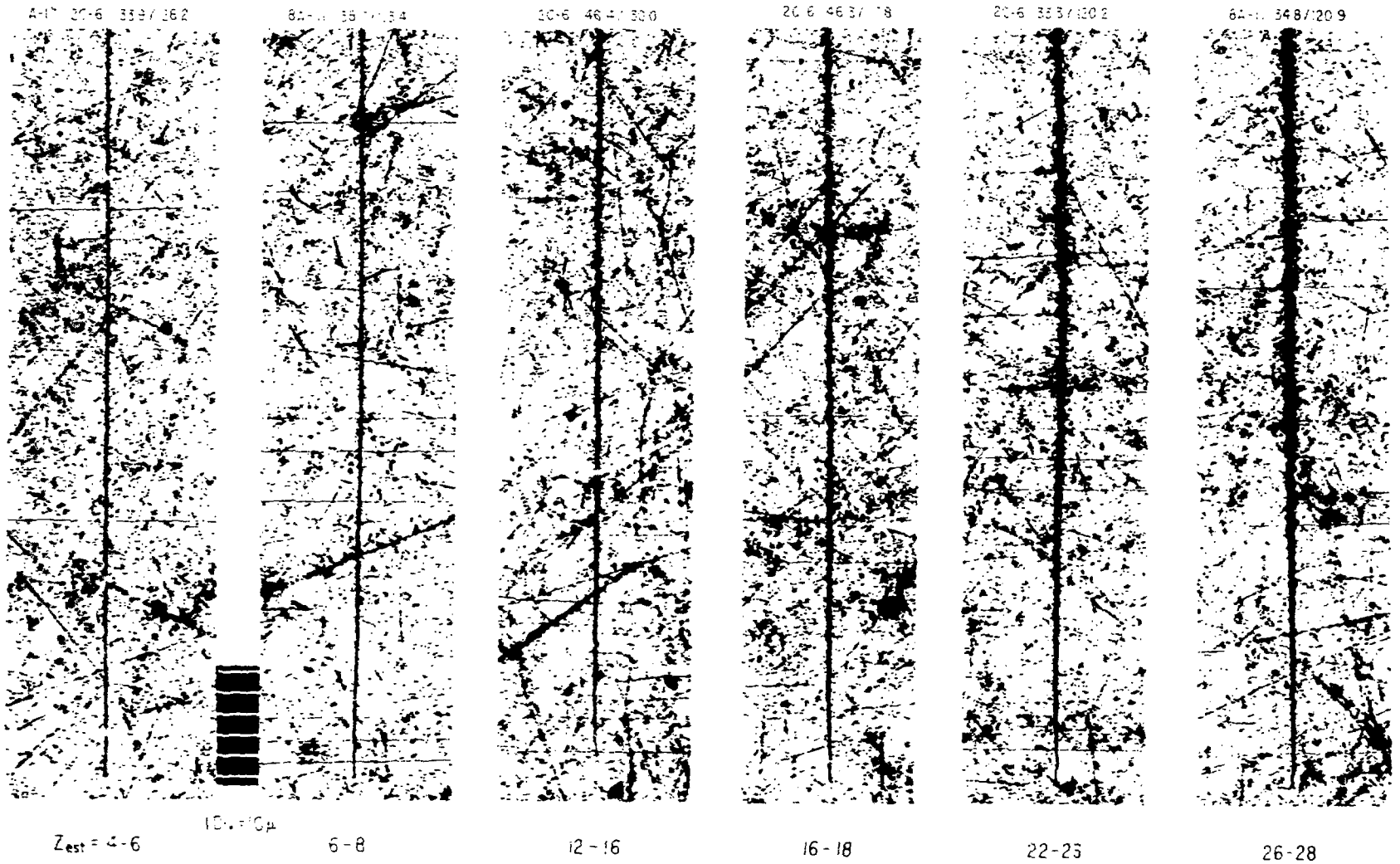

Terminal Sections of HZE Particle Tracks in Ilford K.2 Emulsion Flown on Apollo 17

Figure 13

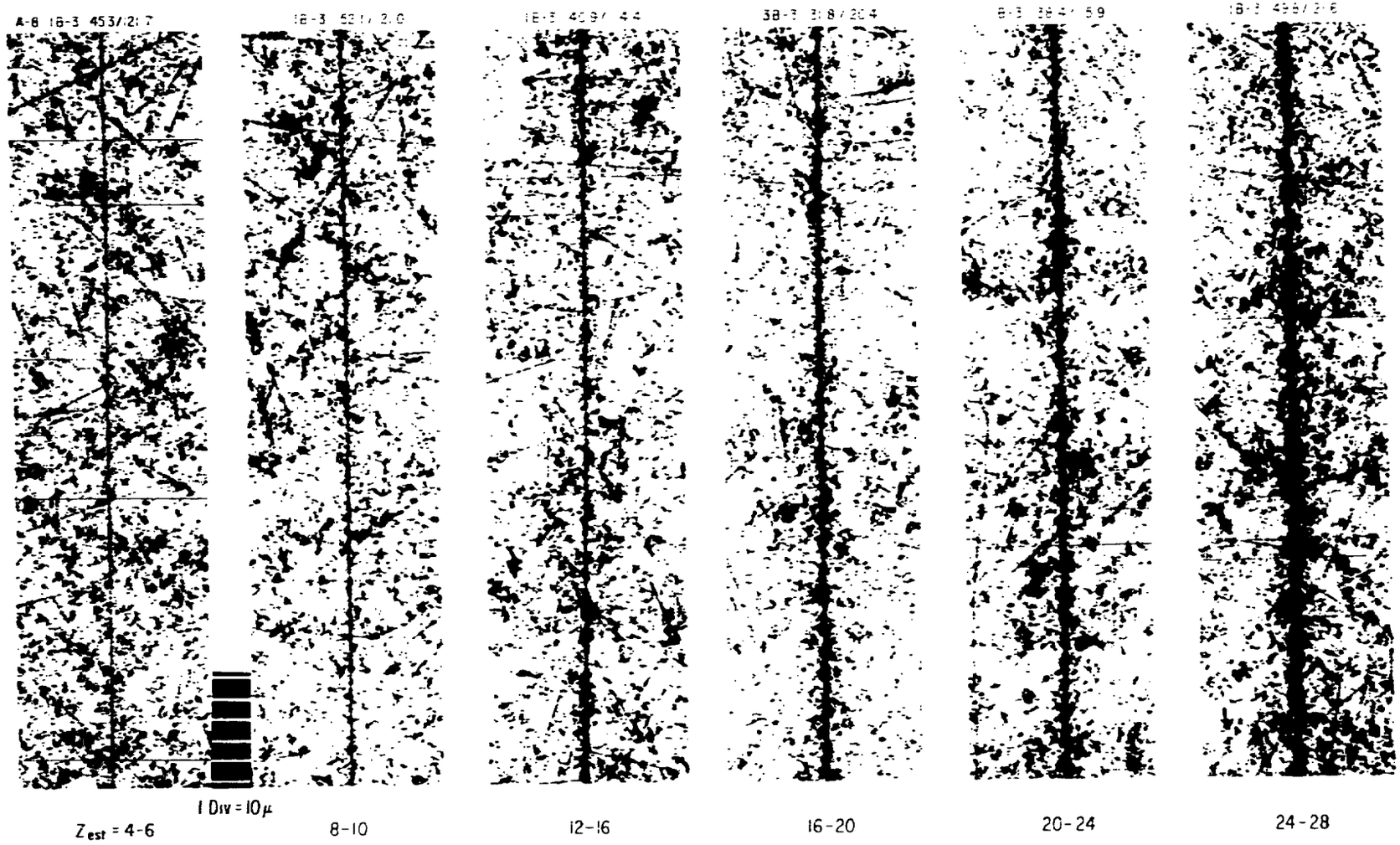

High Energy Sections of HZE Particle Tracks in Ilford G.5 Emulsion Flown on Apollo 8

Figure 14

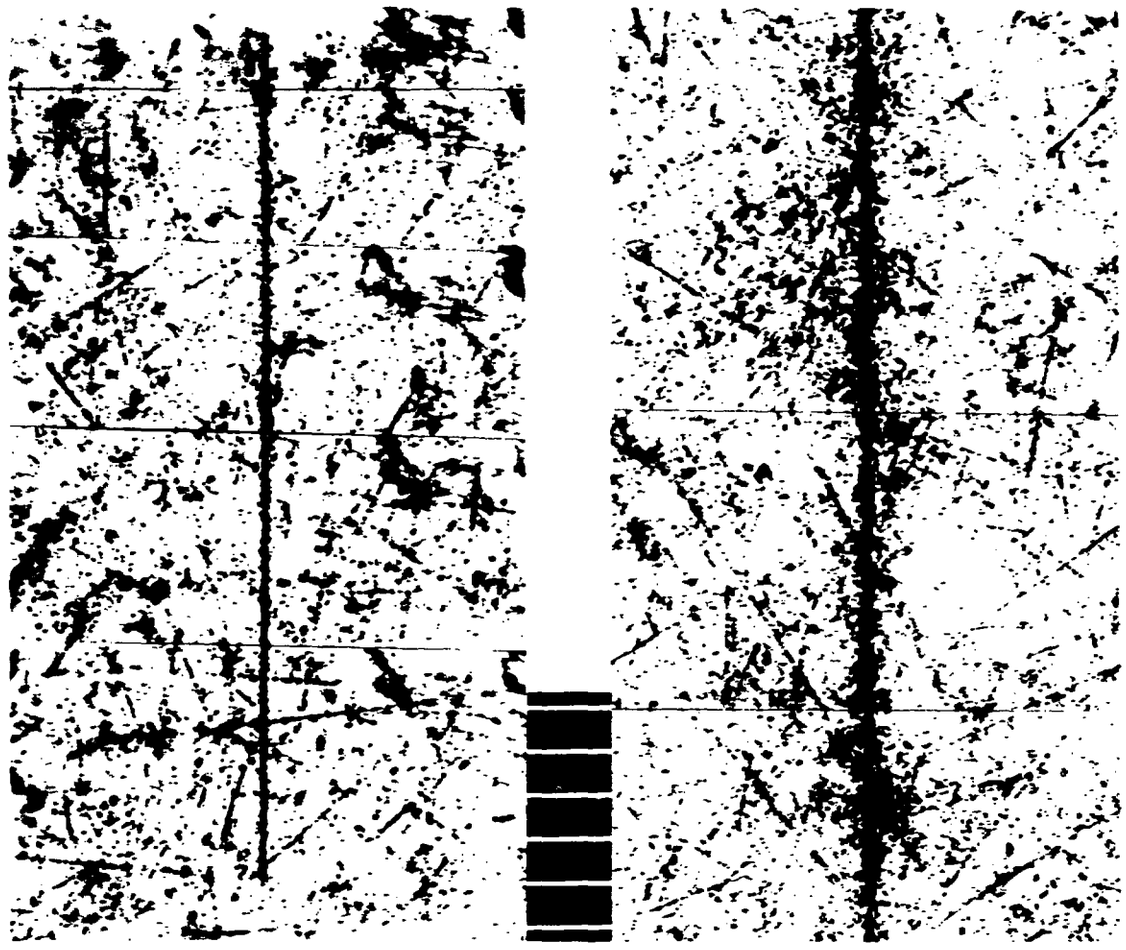

Apollo 17 Film Bag 100μ K.2

Figure 15

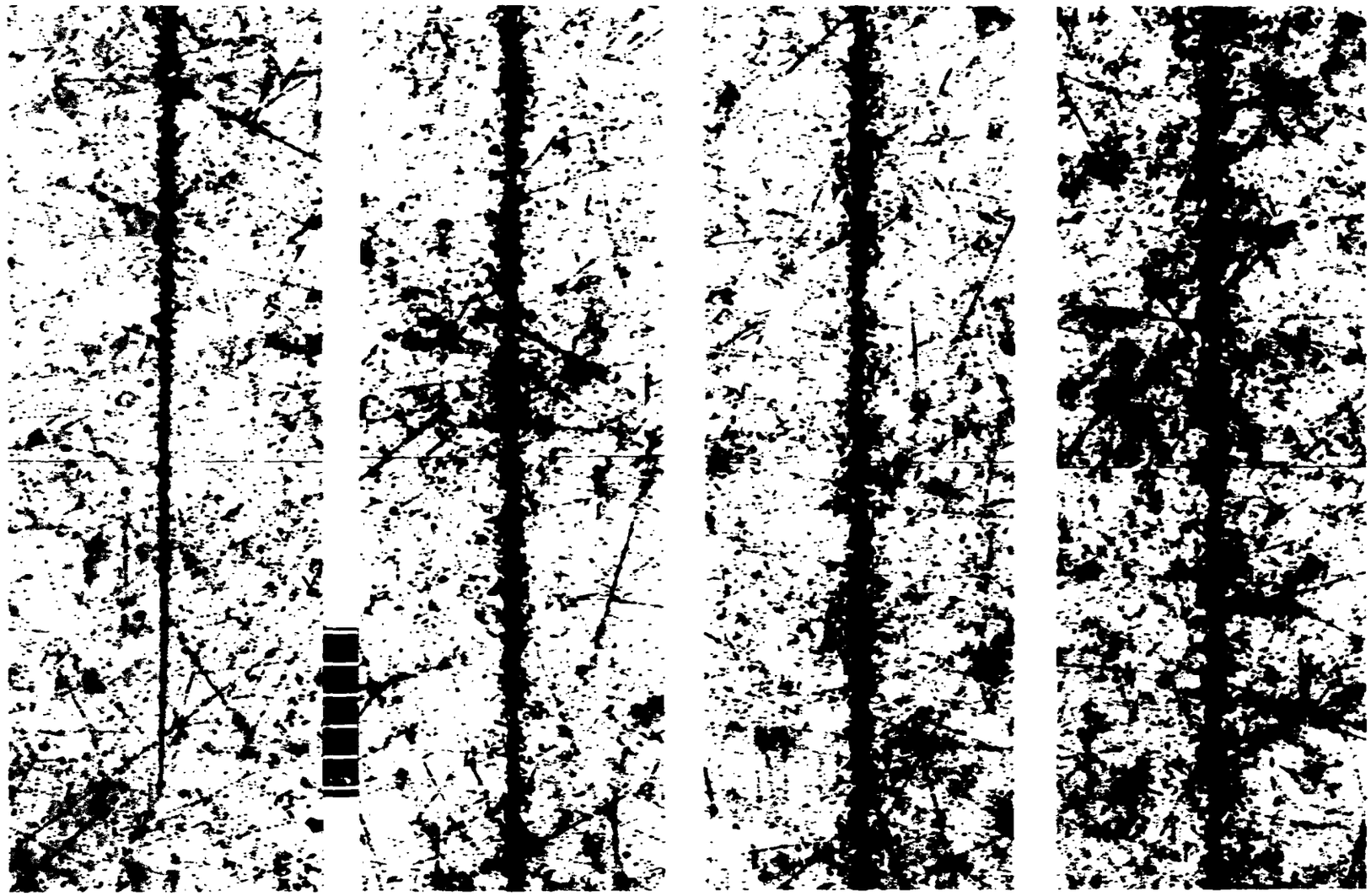

Terminal section of Fe-track (Z=26) in K.2 emulsion carried in film bag on Apollo 17

Figure 16

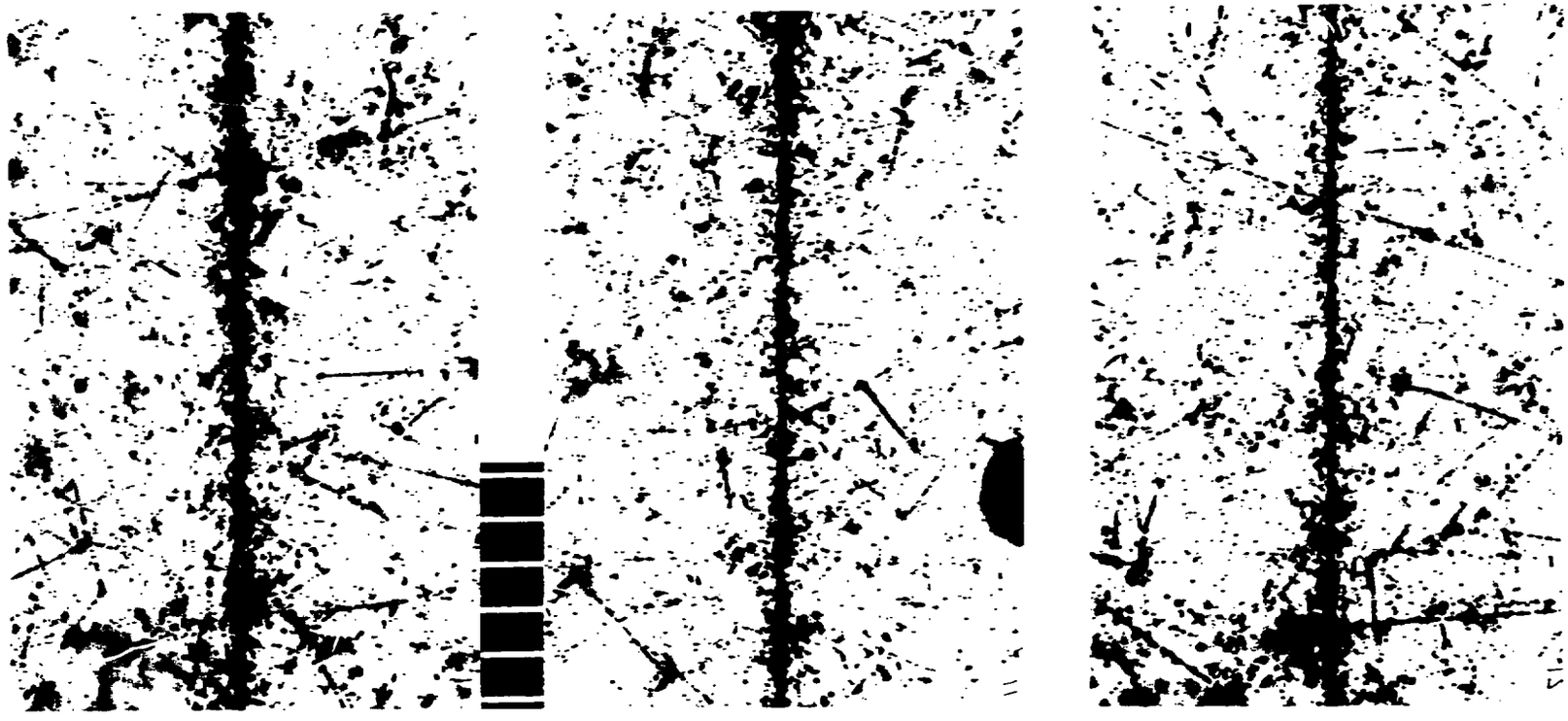

Upbeam sections of Fe-track at selected distances from terminal point

Figure 17

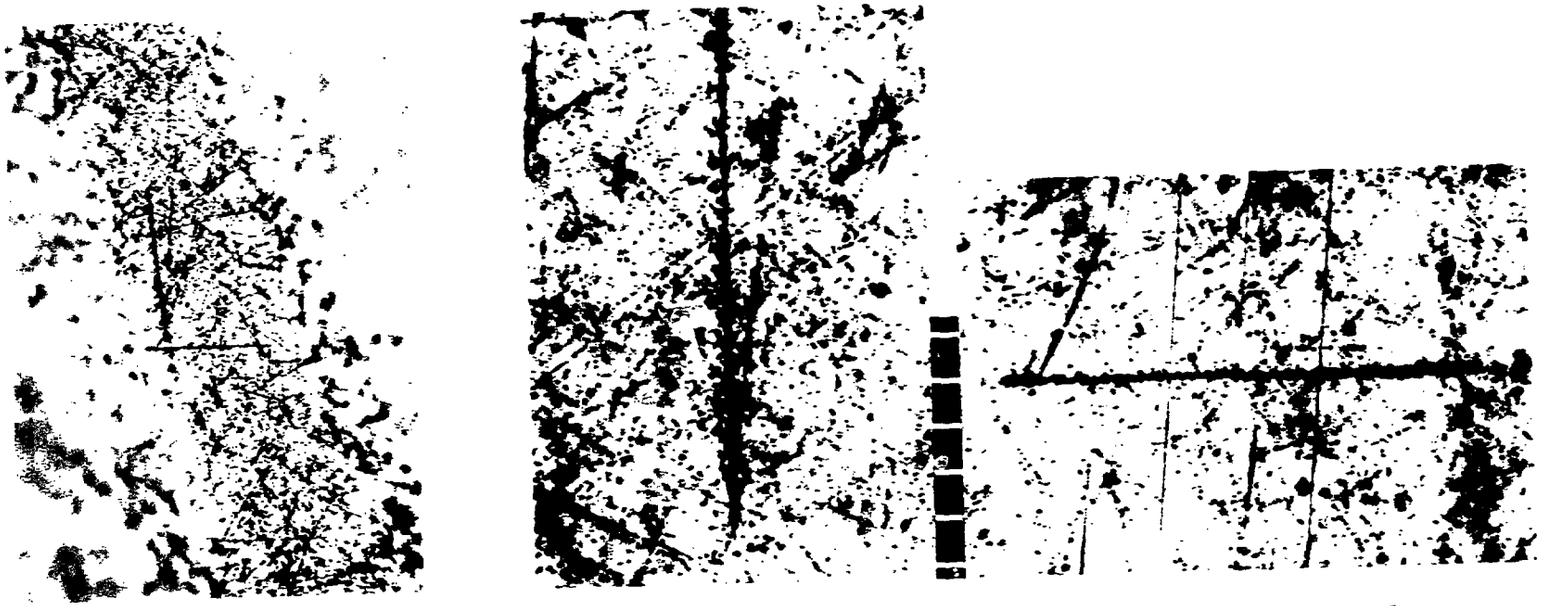

Low-power one-shot and high-power sectional micrographs of 2 HZE particle tracks

45.2/123.1 8B-11 (Biocore) Apollo 17

Figure 18

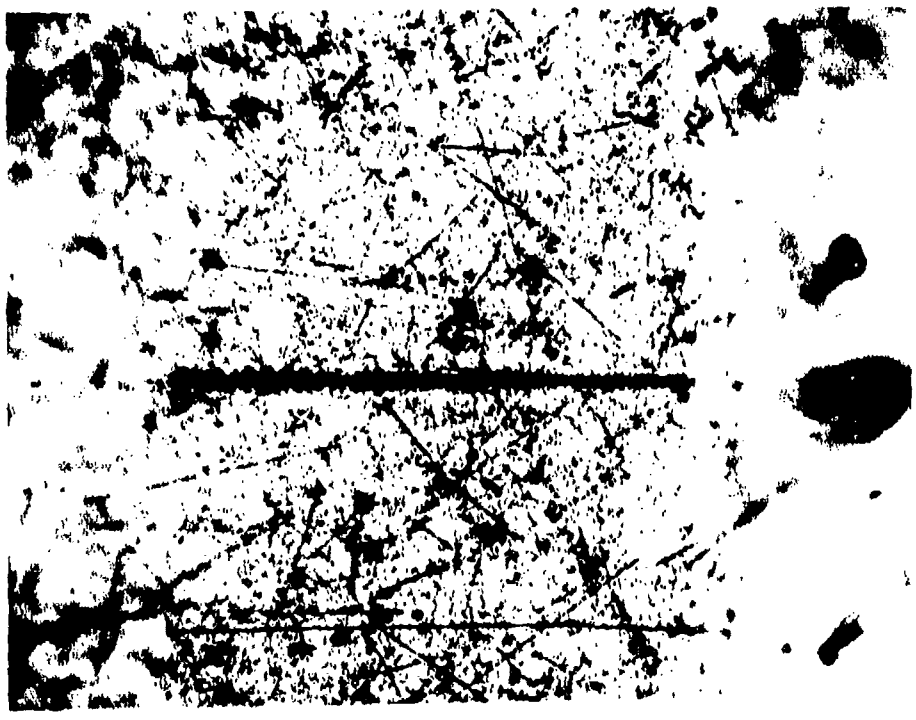

One-shot micrograph of MH pre-thindown
(Em plane tilted against focal plane)

8B-11 (Biocore) 42.5/117.7 Apollo 17

Figure 19

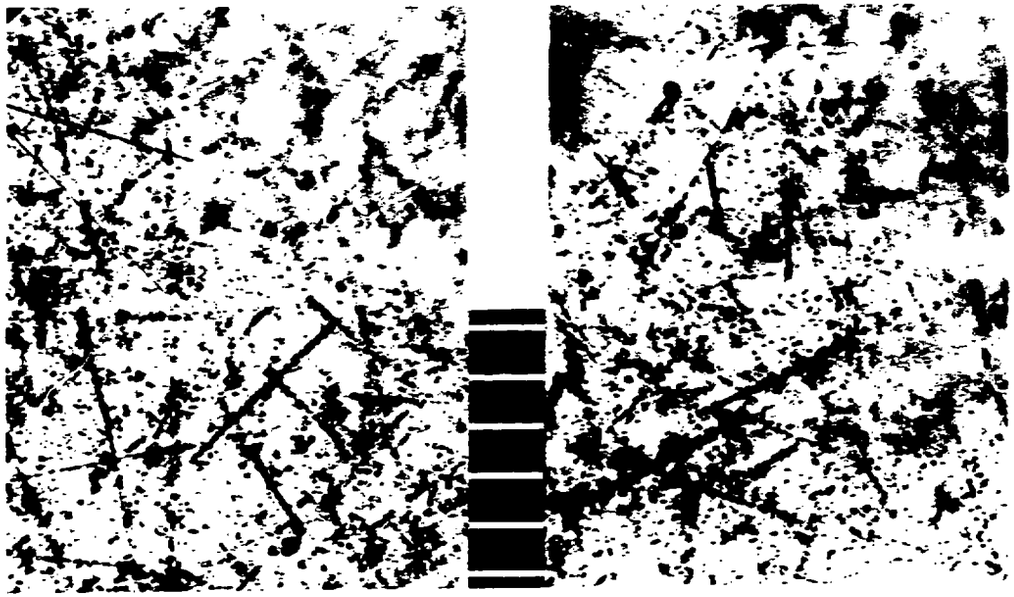

A-17 88-11 29.8/116.9 29.4/112.1

Z_{est} = 8-10 1 Div. = 10 μ Z_{est} = >20

Apollo 17 Biocore 100μ K.2

Highly Tilted Thindowns

Figure 20

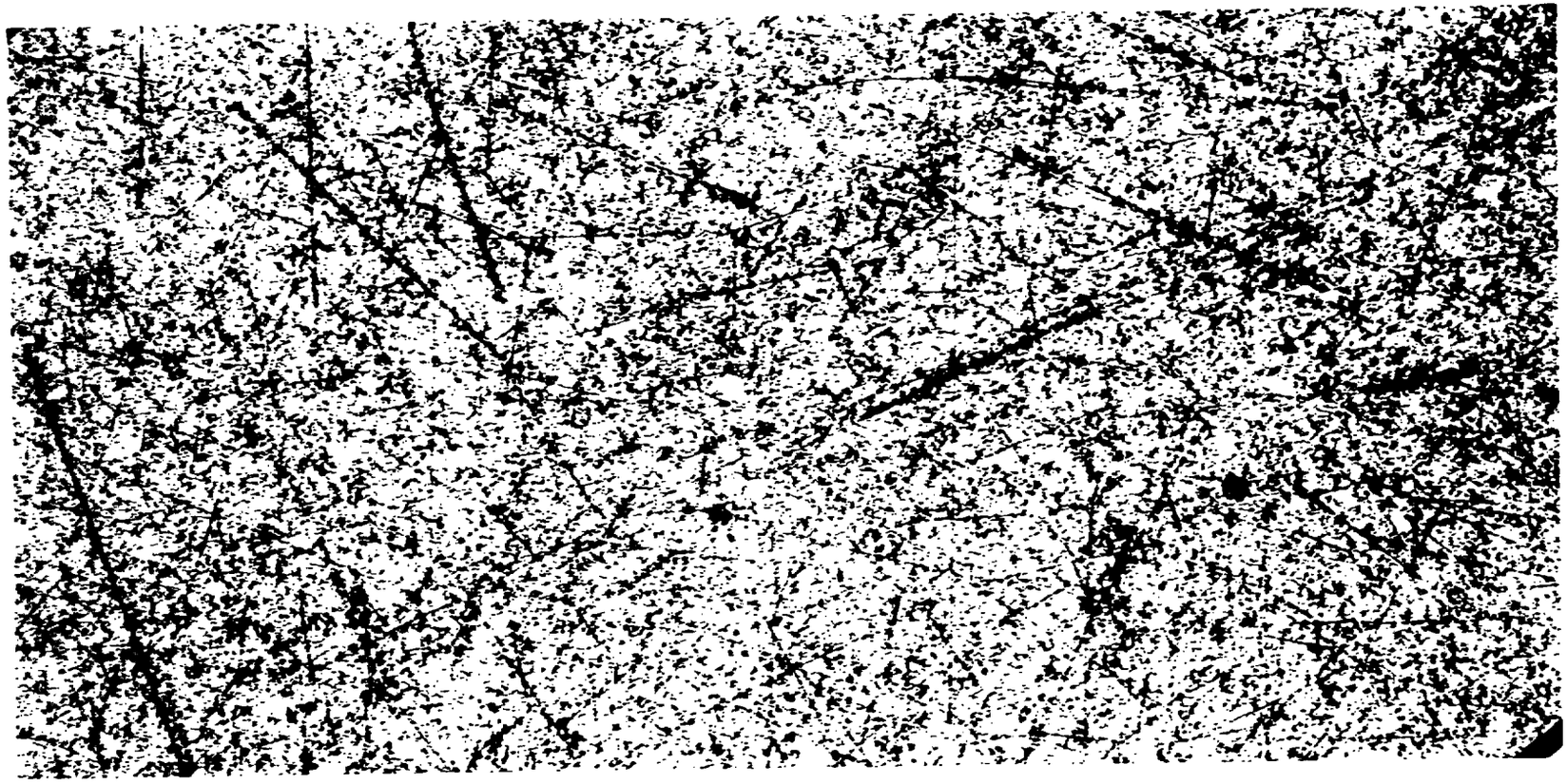

Low - power panorama of K.2 emulsion

4C-6 (CDR-A) on Apollo 17

Figure 21

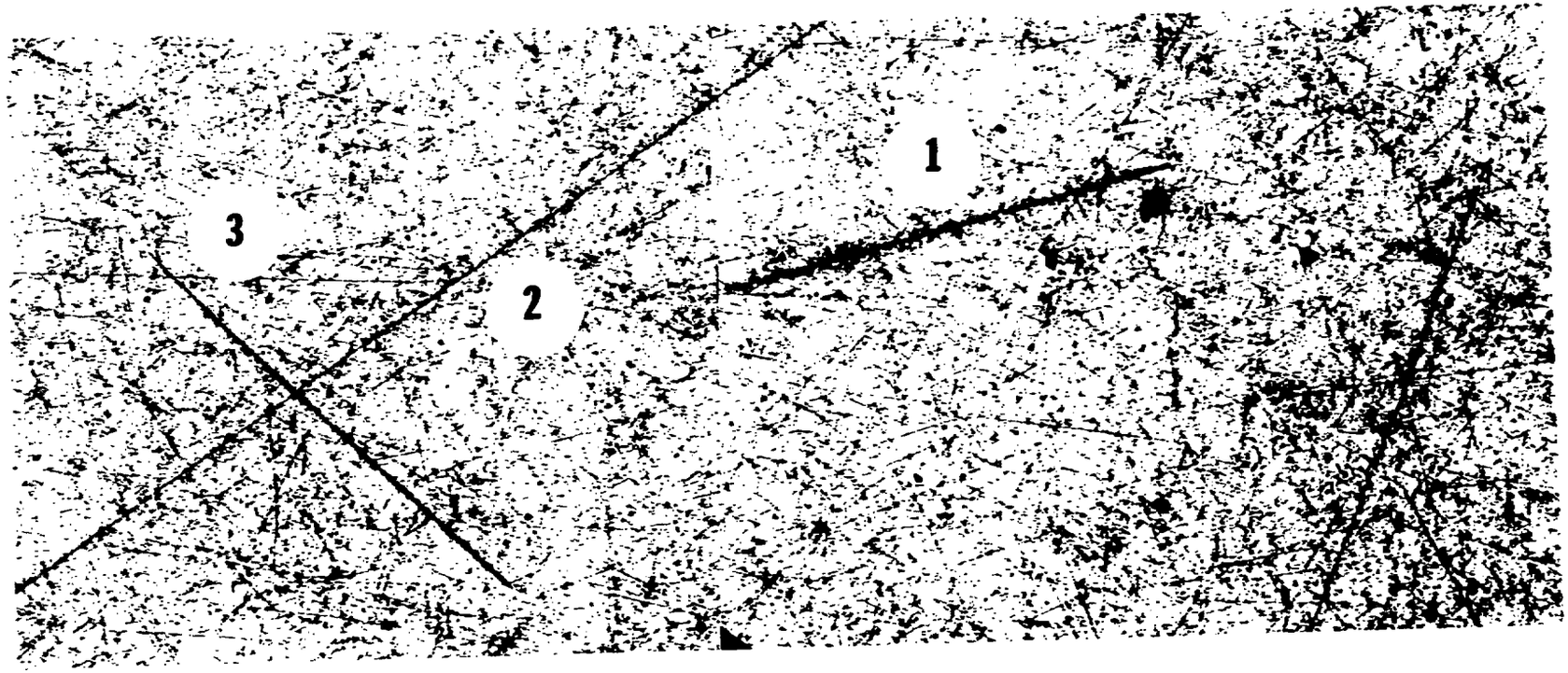

Low - power panorama of K.2 emulsion

3C-2 (CMP-A) on Apollo 17

Figure 22

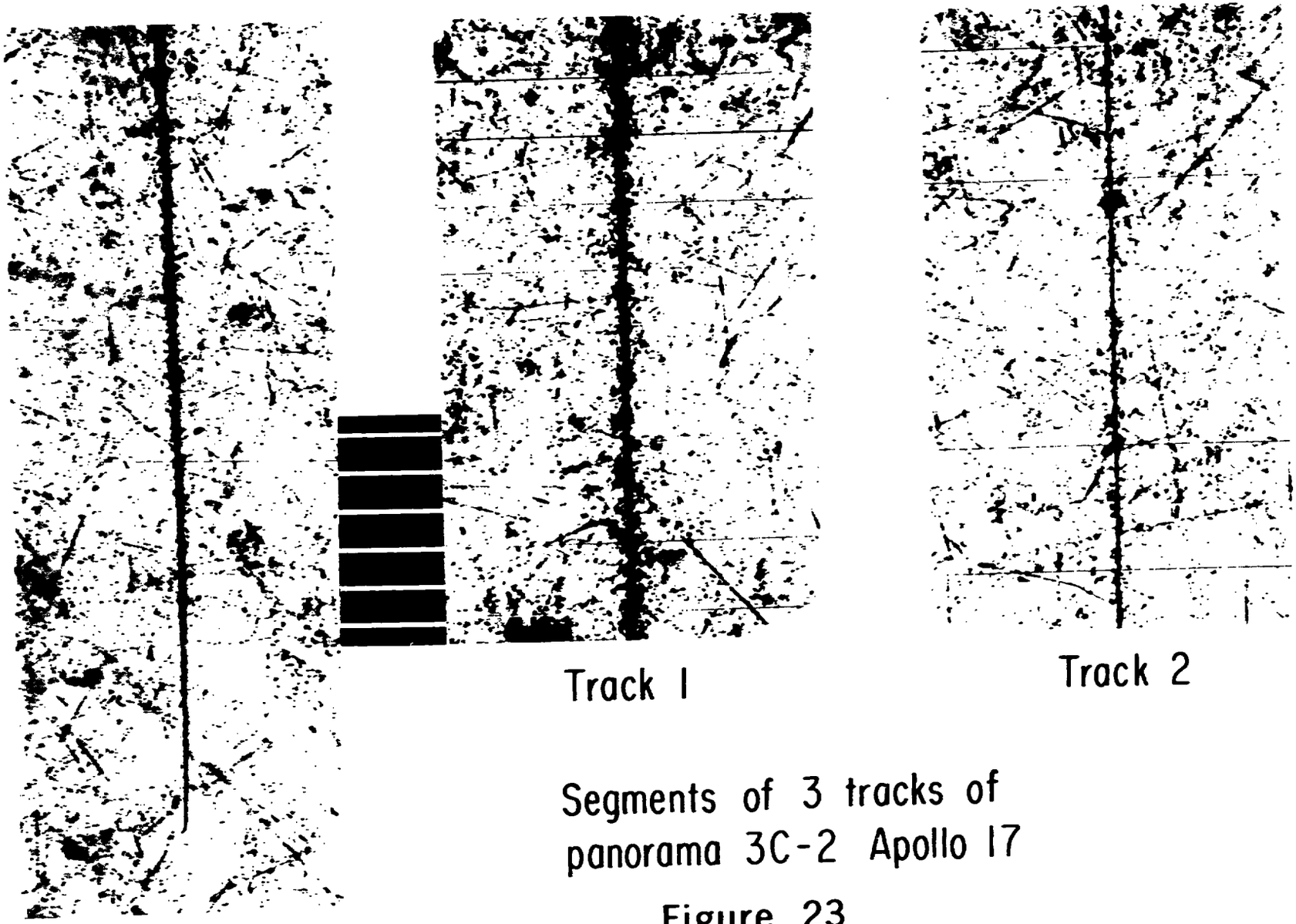

Track 3

Track 1

Track 2

Segments of 3 tracks of
panorama 3C-2 Apollo 17

Figure 23

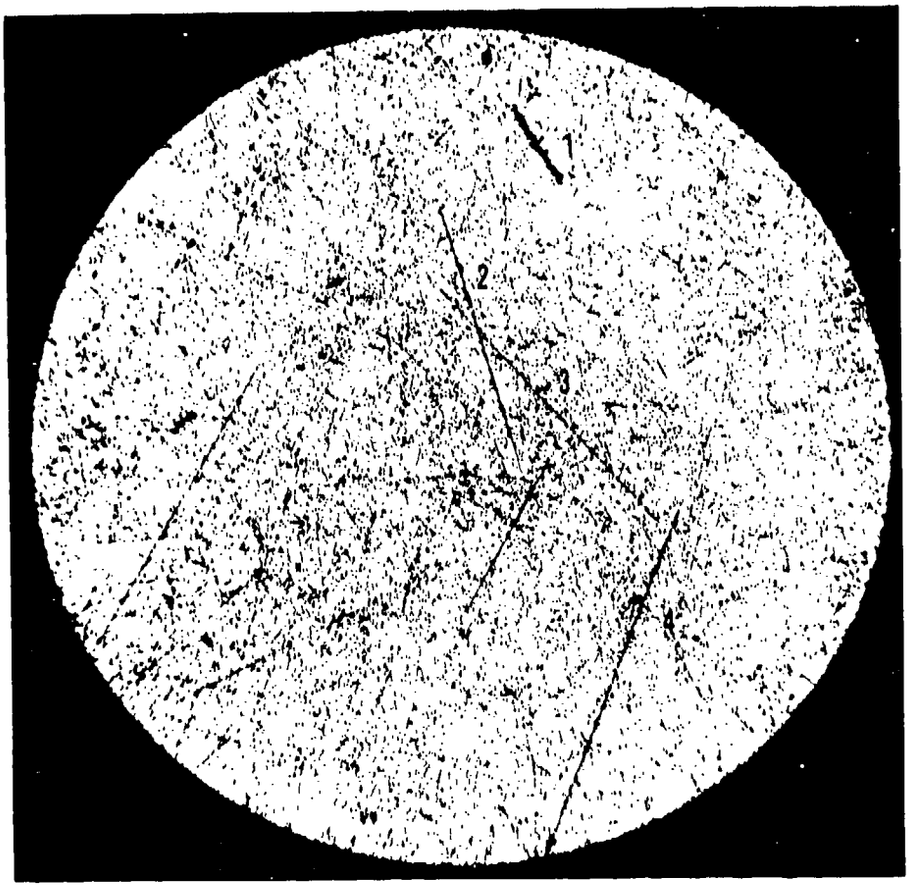

8A-11 (Film bag) 43.0/122.6 Apollo 17

Figure 24

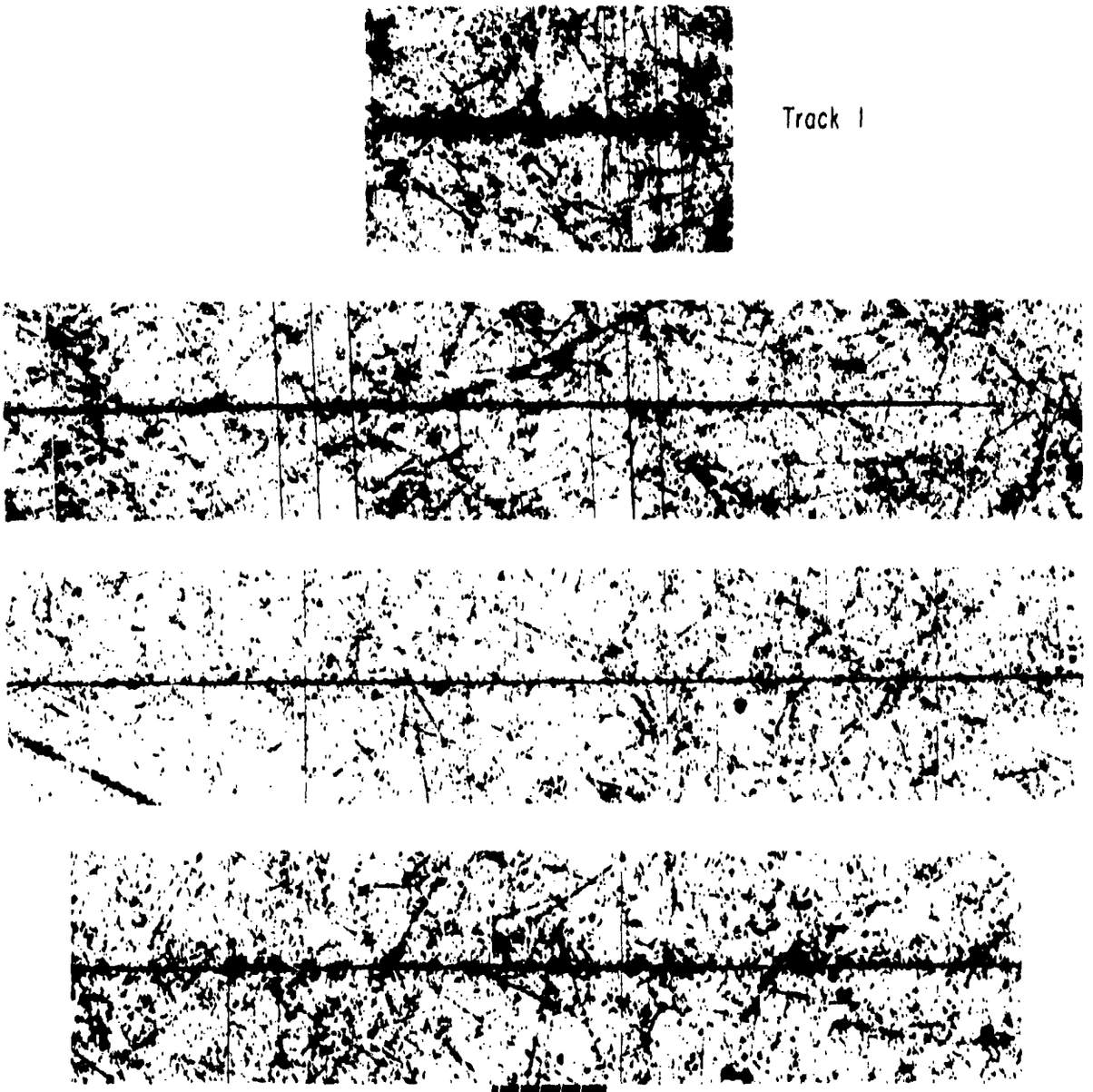

Segments of 4 Tracks of Low-Power Survey 8A-11 Apollo 17

Figure 25

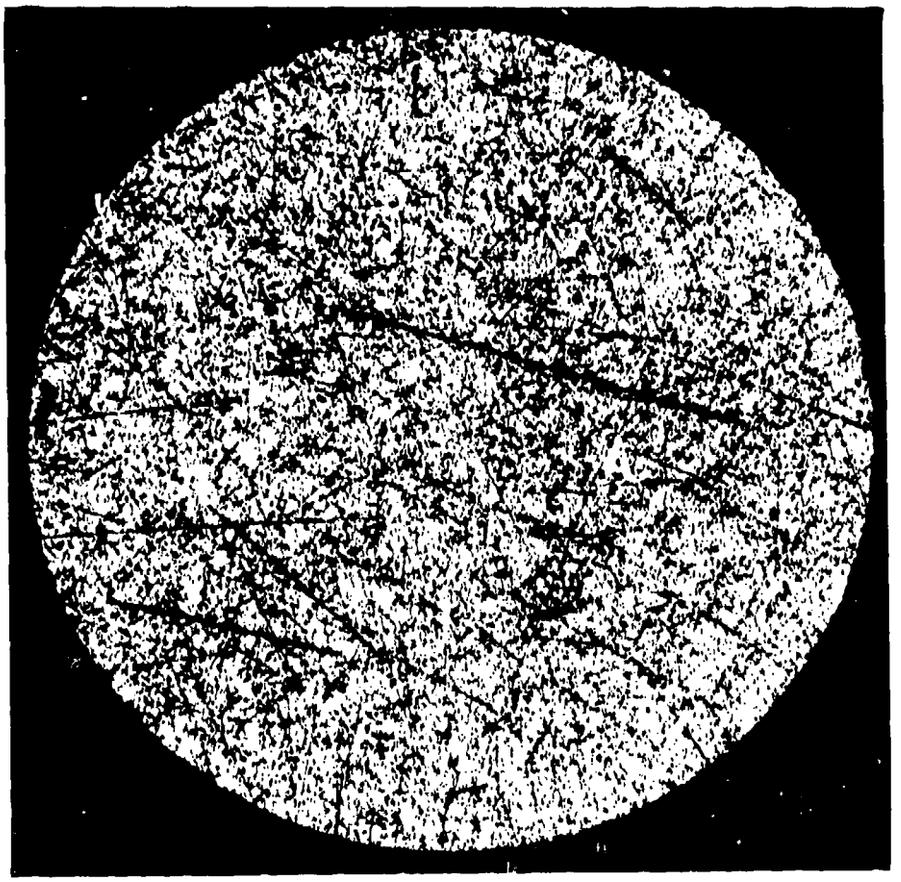

Low power visual field with several HZE particle tracks

4C-6 (CDR-A) 28.2/118.7 Apollo 17

Figure 26

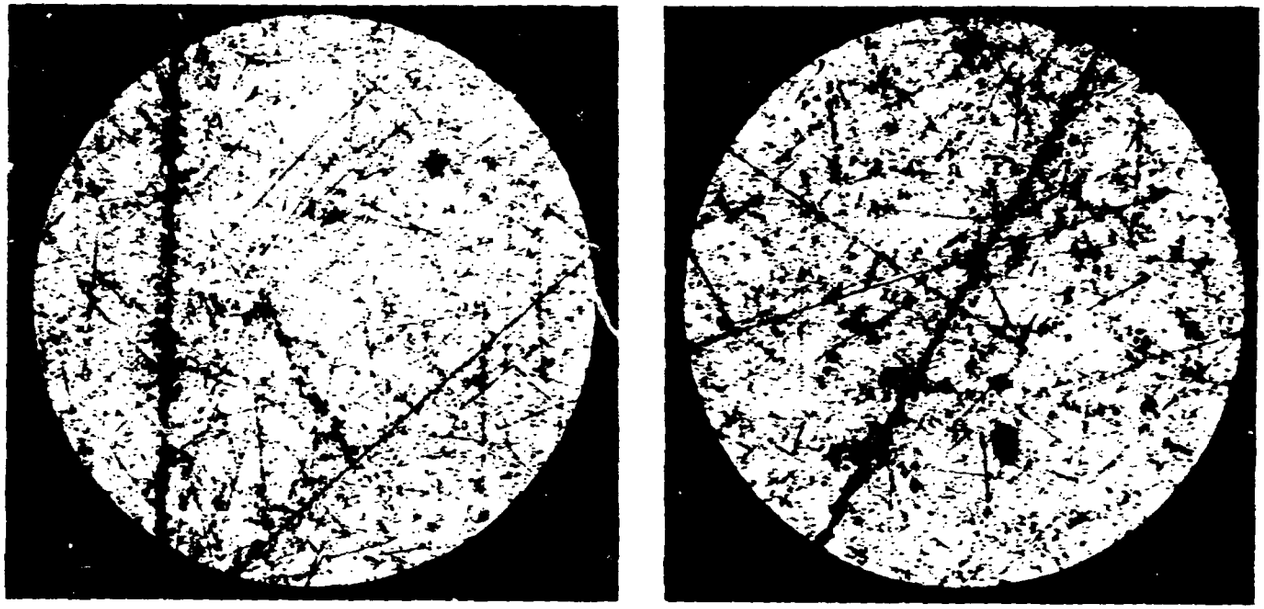

48.6/113.0 35.5/125.9

High power visual fields

8A-1 (Film bag) Apollo 17

Figure 27

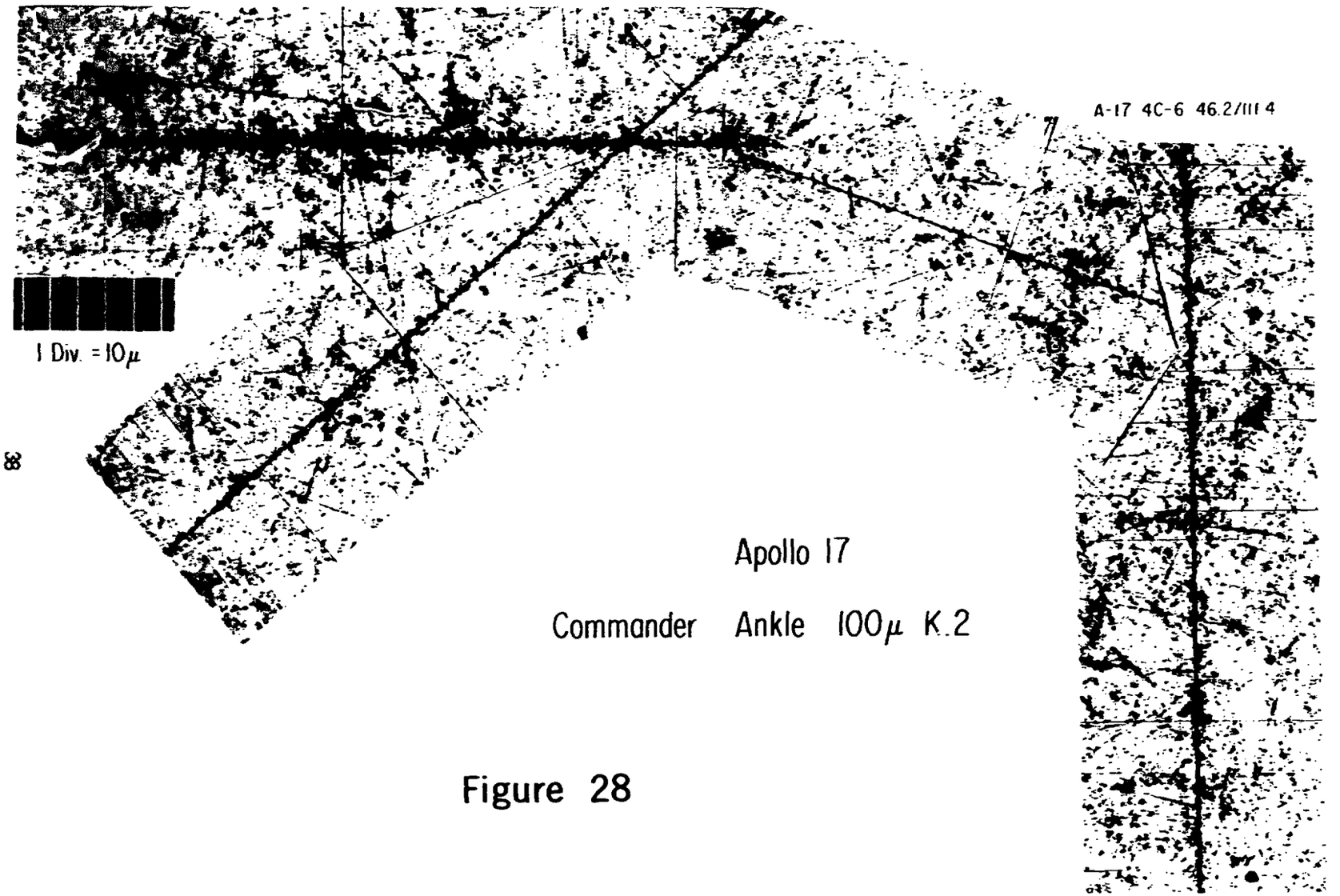

Apollo 17

Commander Ankle 100μ K.2

Figure 28

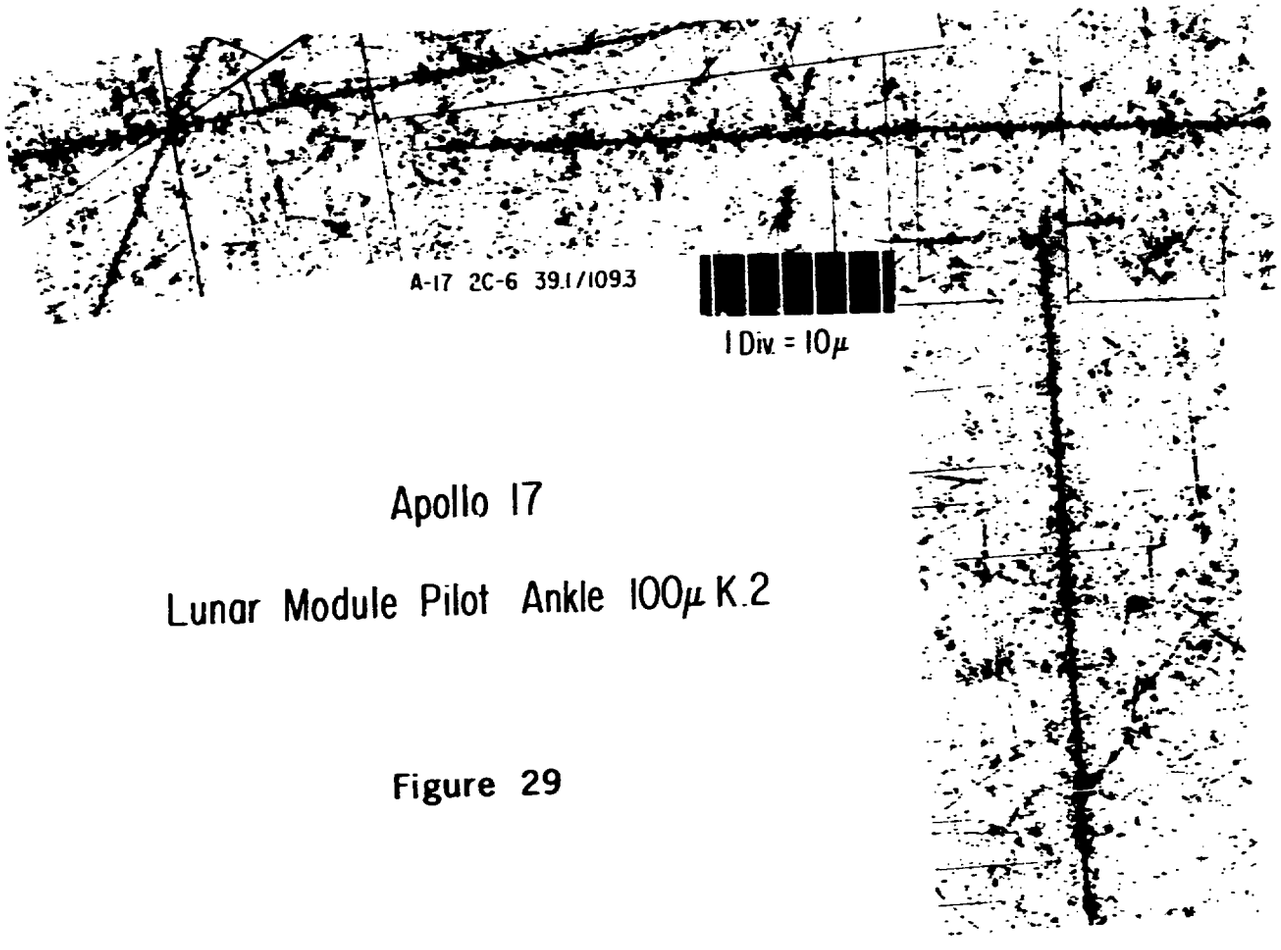

Apollo 17

Lunar Module Pilot Ankle 100μ K.2

Figure 29

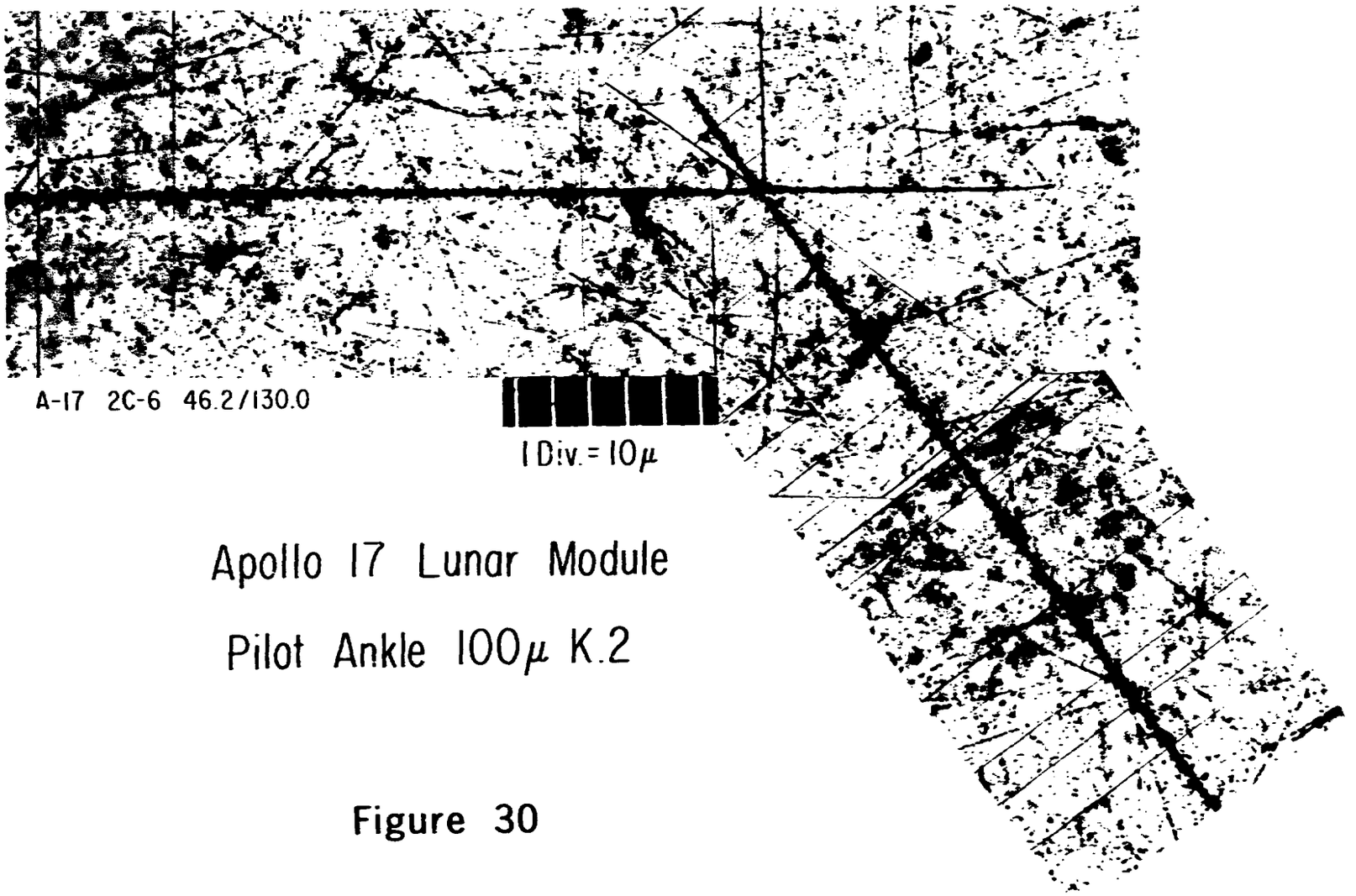

Apollo 17 Lunar Module

Pilot Ankle 100μ K.2

Figure 30

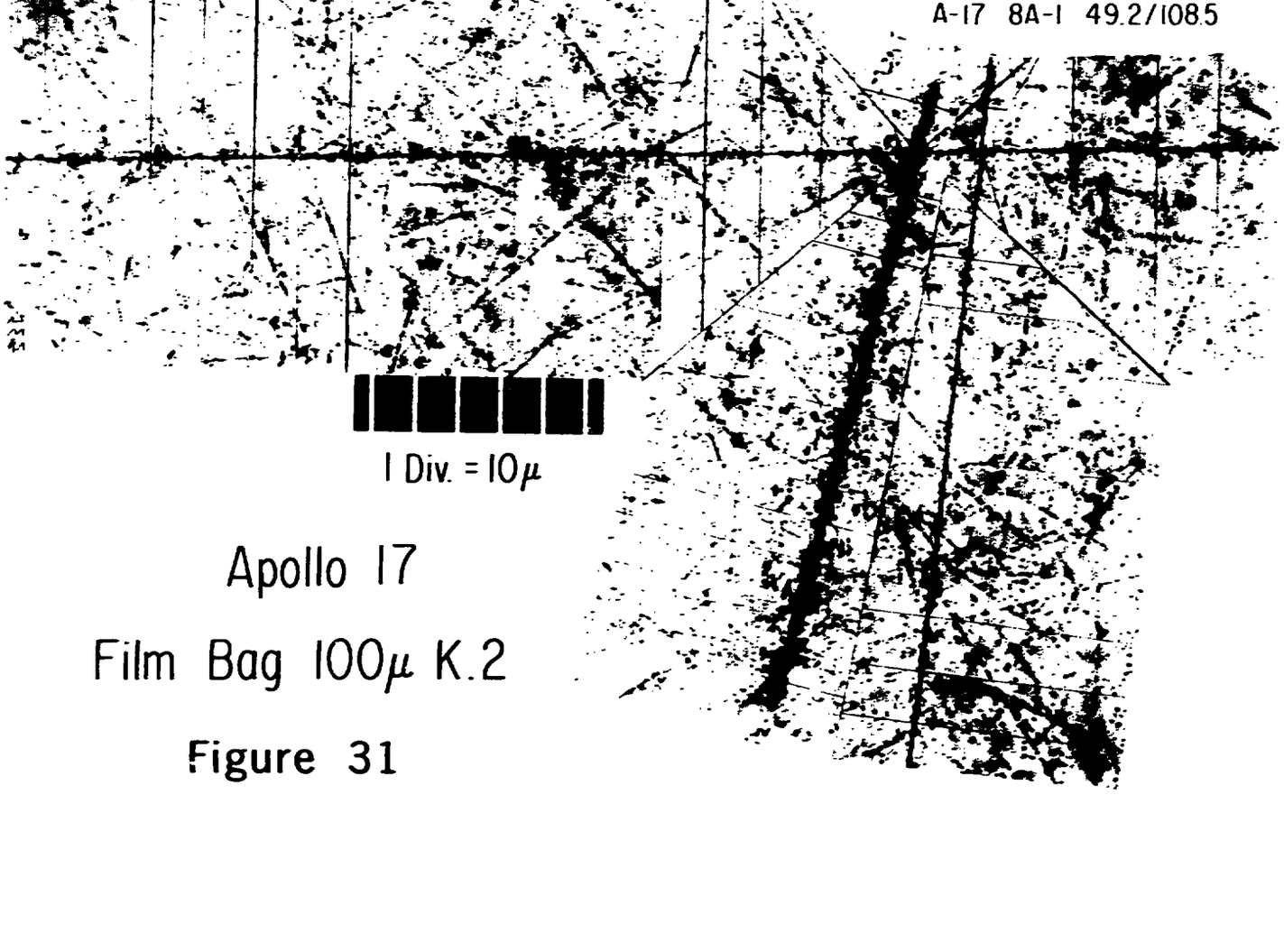

Apollo 17

Film Bag 100μ K.2

Figure 31

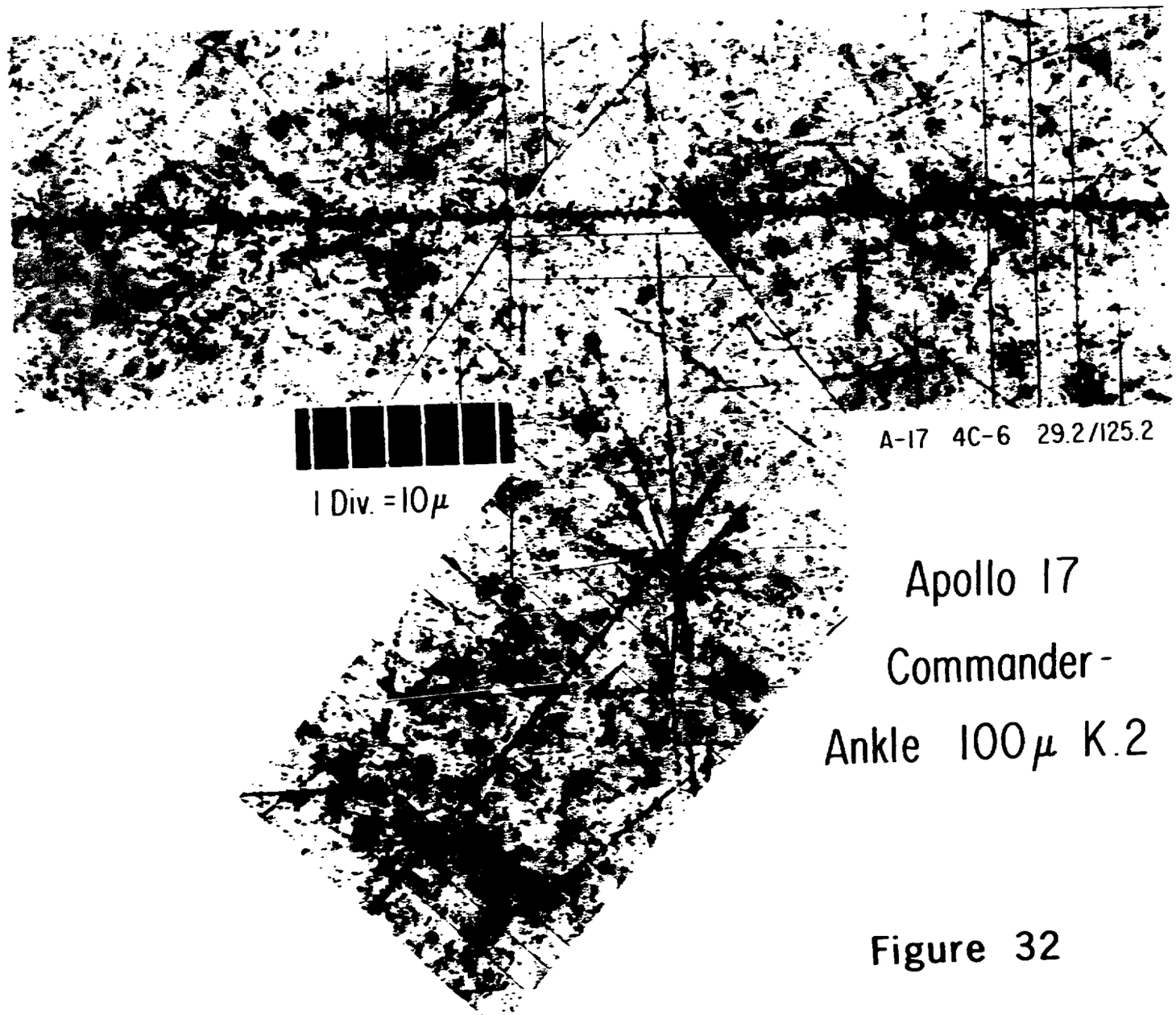

Apollo 17

Commander -

Ankle 100μ K.2

Figure 32

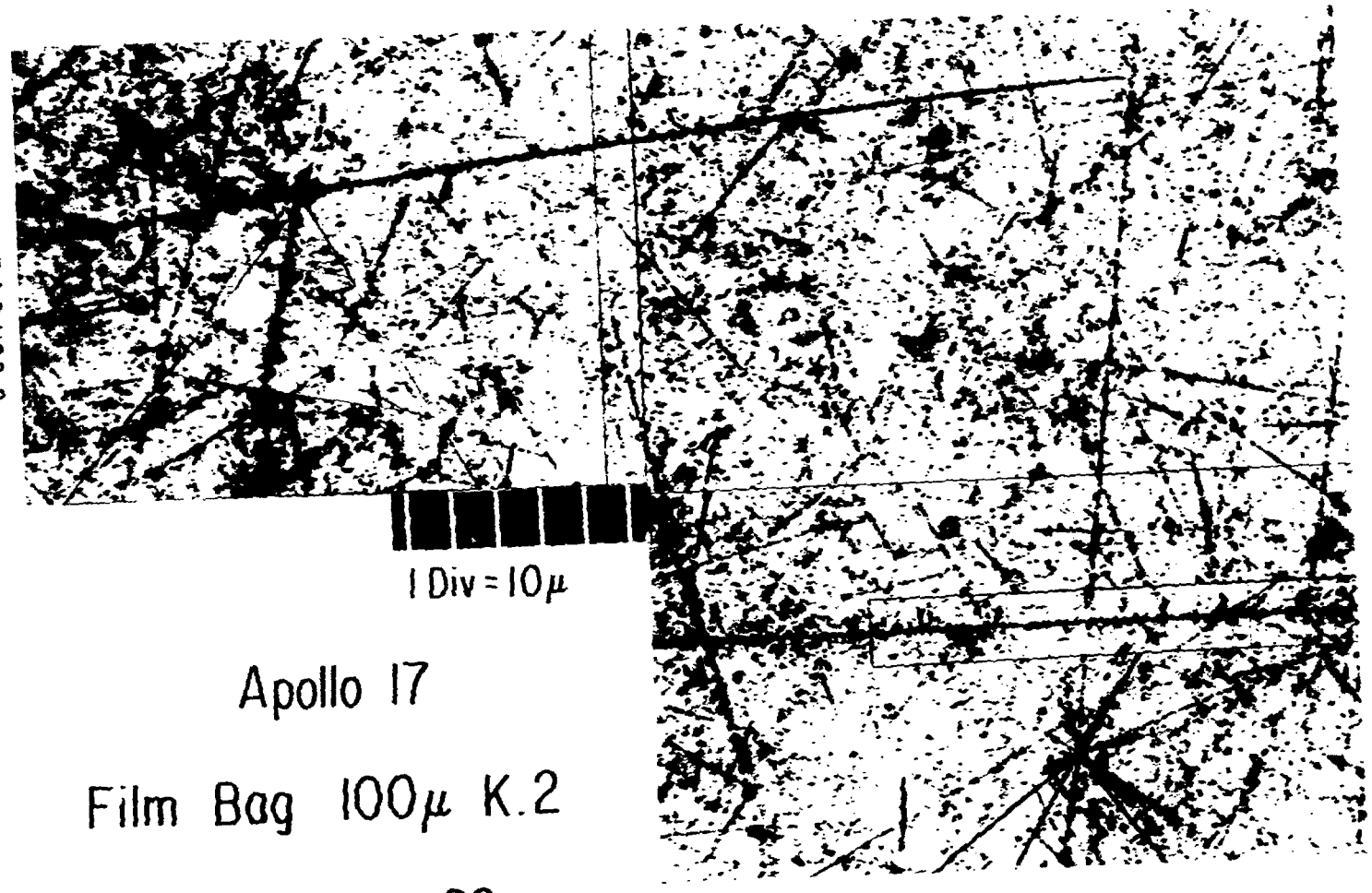

Apollo 17

Film Bag 100μ K.2

Figure 33

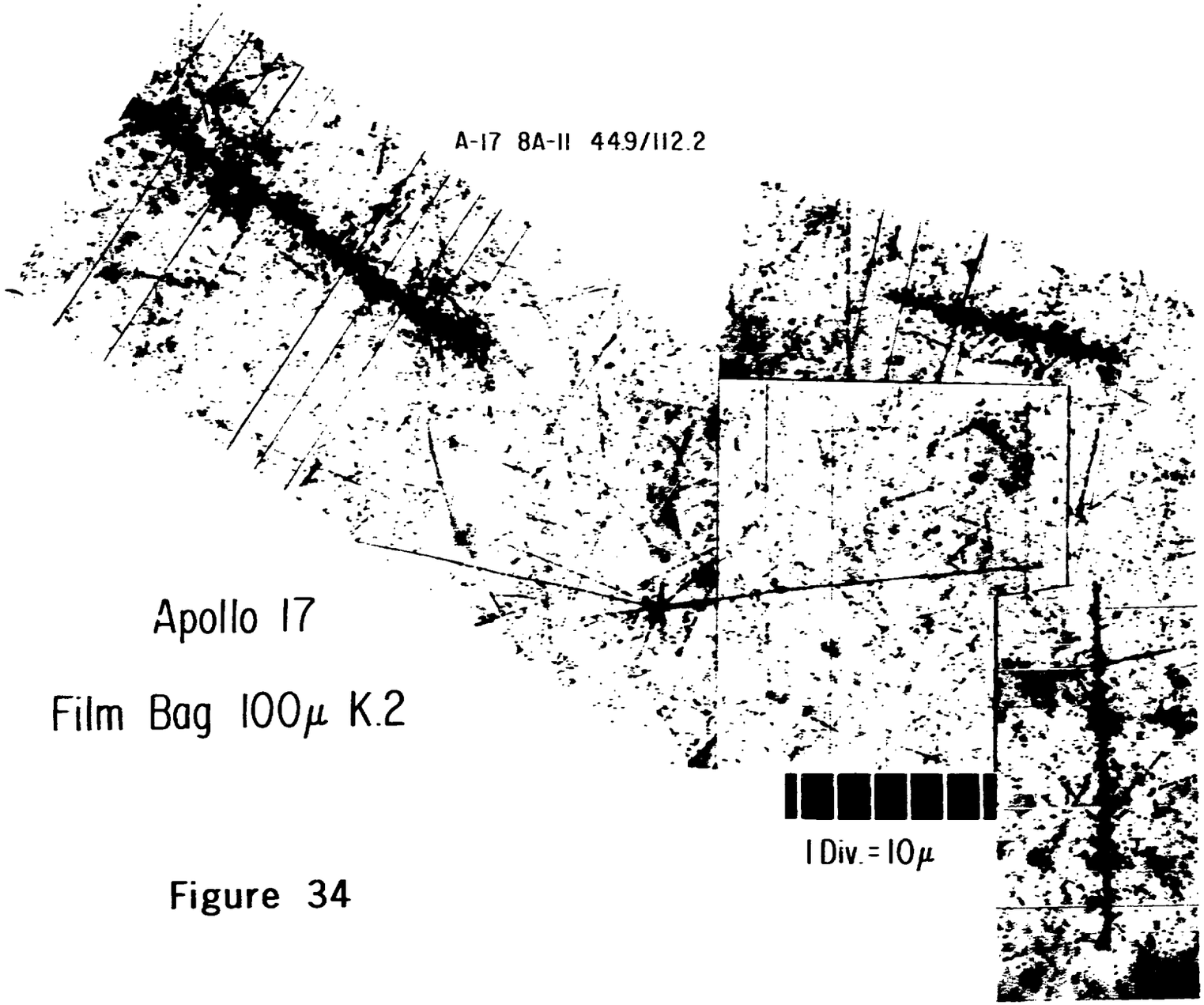

Apollo 17

Film Bag 100μ K.2

Figure 34

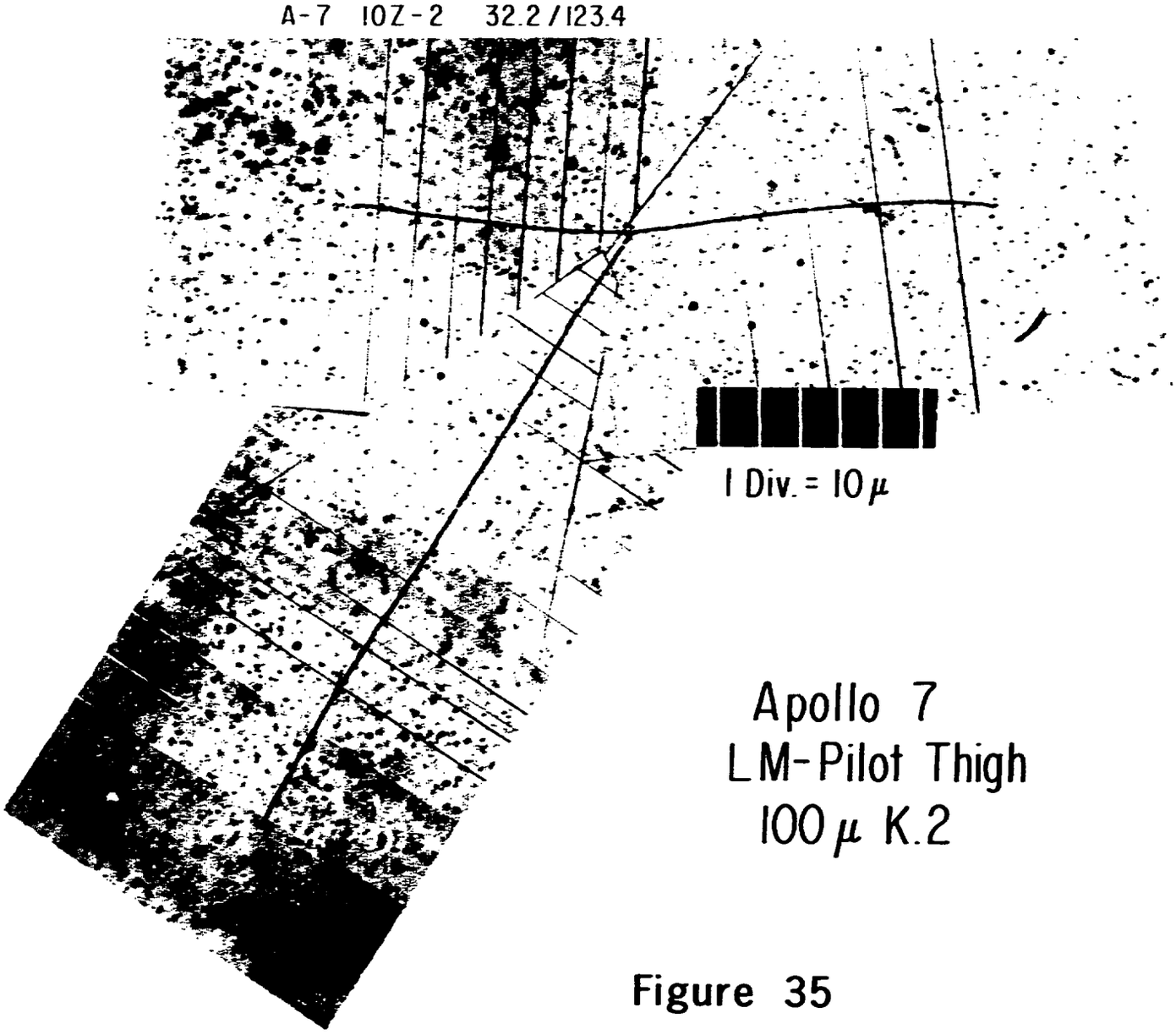

Apollo 7
LM-Pilot Thigh
100 μ K.2

Figure 35

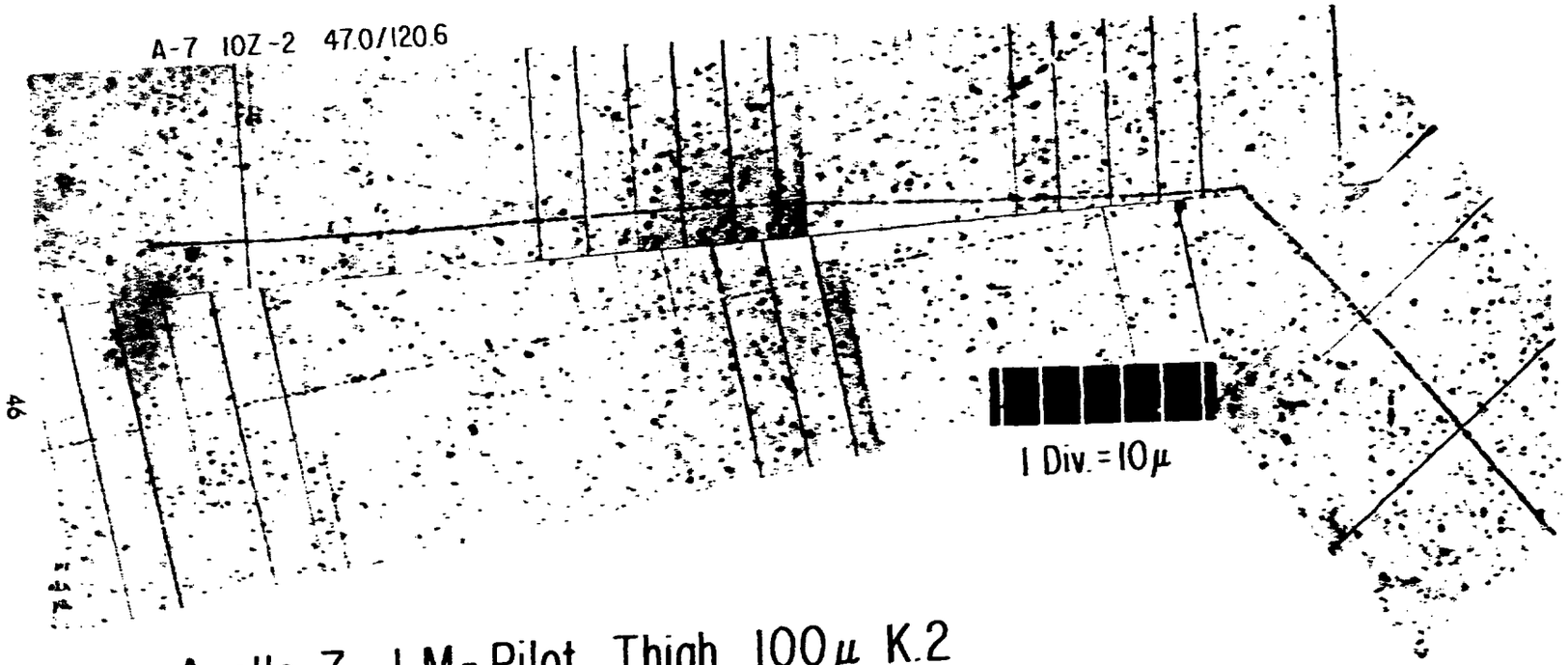

Apollo 7 LM-Pilot, Thigh 100μ K.2

Figure 36

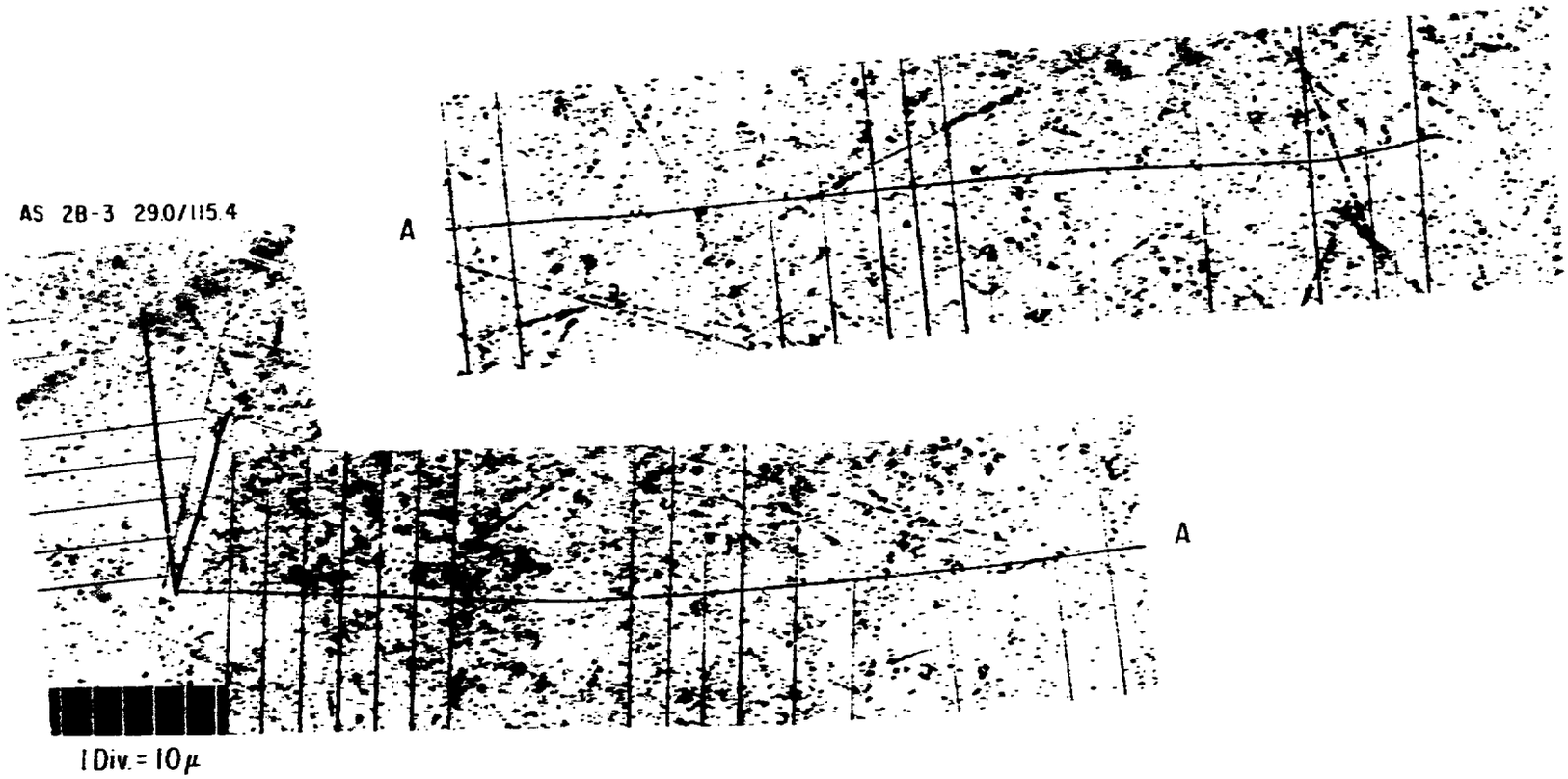

Apollo - Soyuz C-Pilot 100μ K.2

Figure 37

UNCLASSIFIED
Security Classification

DOCUMENT CONTROL DATA - R & D

Security classification of title, body of abstract and indexing annotation must be entered when the overall report is classified)

1. ORIGINATING ACTIVITY (Corporate author)
Naval Aerospace Medical Research Laboratory
Pensacola, Florida 32508

2a. REPORT SECURITY CLASSIFICATION
Unclassified

2b. GROUP
N/A

3. REPORT TITLE
ATLAS OF NUCLEAR EMULSION MICROGRAPHS FROM PERSONNEL DOSIMETERS OF MANNED SPACE MISSIONS

4. DESCRIPTIVE NOTES (Type of report and inclusive dates)
N/A

5. AUTHOR(S) (First name, middle initial, last name)
Hermann J. Schaefer and Jeremiah J. Sullivan

6. REPORT DATE	7a. TOTAL NO. OF PAGES	7b. NO. OF REFS
27 May 1976	47	14

8a. CONTRACT OR GRANT NO	9a. ORIGINATOR'S REPORT NUMBER(S)
NASA Order No. T-3057-C	
b. PROJECT NO	
c.	9b. OTHER REPORT NO(S) (Any other numbers that may be assigned this report)
d.	

10. DISTRIBUTION STATEMENT
Approved for public release; distribution unlimited.

11. SUPPLEMENTARY NOTES	12. SPONSORING MILITARY ACTIVITY
Prepared for the Lyndon B. Johnson Space Center of NASA.	

13. ABSTRACT

A collection of micrographs is presented taken from nuclear emulsions of personnel dosimeter packs carried by the astronauts on near-Earth orbital and lunar missions. It is intended as a pictorial record and illustration of the radiation environment in space and as a supplement to earlier reports and publications of the laboratory in which the emulsion findings have been presented in detail for individual missions. A complete list of those earlier accounts procedes the picture section.

DD FORM 1 NOV 65 1473 (PAGE 1)
S/N 0101-807-6801

UNCLASSIFIED
Security Classification

14 KEY WORDS	LINK A		LINK B		LINK C	
	ROLE	WT	ROLE	WT	ROLE	WT
Personnel radiation monitoring in space						
Nuclear emulsion micrographs of the astronaut's radiation exposure						